Quantum Hall effect in silicon metal-oxide-semiconductor inversion layers: Experimental conditions for determination of h/e^2

Kazuo Yoshihiro, Joji Kinoshita, Katsuya Inagaki, and Chikako Yamanouchi
Device Fundamentals Section, Electrotechnical Laboratory, Sakura-mura, Niihari-gun, Ibaraki 305, Japan

Tadashi Endo, Yasushi Murayama, and Masao Koyanagi
Quantum Metrology Section, Electrotechnical Laboratory, Sakura-mura, Niihari-gun, Ibaraki 305, Japan

Atsuo Yagi
Semiconductor Group, Sony Corporation, Atsugi, Kanagawa 243, Japan

Jun-ichi Wakabayashi and Shinji Kawaji
Department of Physics, Gakushuin University, Mejiro, Toshima-ku, Tokyo 171, Japan
(Received 18 June 1985)

High-precision measurements of quantum Hall and diagonal resistivities have been made for a number of silicon metal-oxide-semiconductor field-effect transistor samples at temperatures from 1.4 to ~ 0.5 K, magnetic inductions from 9.0 to ~ 15 T, and channel currents up to $\sim 20\ \mu A$. The concentration of two-dimensional electrons was changed from 8.6×10^{15} to $4.0\times 10^{16}\ m^{-2}$. When the measurement is made under the condition that $\rho_{xx} < (4/i)\times 10^{-2}\ \Omega$ holds for the ith quantized Hall plateau, the Hall resistivity ρ_{xy} is verified to be constant, i.e., the value corresponding to h/e^2 is unchanged against changes in electron concentration, temperature, magnetic field strength, and channel current, to within one part in 10^7, the accuracy of the present experiment. The tentative result and its one-standard-deviation uncertainty are $(i/4)\overline{R}_H(i) = 6453.2009 \pm 0.0022\ \Omega_{ETL}$ (0.34 ppm) referred to the ohm as maintained by the Electrotechnical Laboratory in Ibaraki, Japan. The systematic uncertainty associated with Ω_{ETL} has been found to be open to discussion. The effect of dissipative regions distributed over the electron channel is discussed: It could become appreciable in the determination of h/e^2 with an uncertainty of less than a few parts in 10^8. The technique of the present precision measurement can be utilized for experimental studies aimed at solving the most basic problems of transport phenomena at lowest excitations.

I. INTRODUCTION

It is now well known that a typical two-dimensional electron system is realized at the Si-SiO_2 interface of p-type silicon metal-oxide-semiconductor field-effect transistors (MOSFET's) inverted by an electric field perpendicular to the surface,[1] the interface of GaAs-$Al_xGa_{1-x}As$ heterojunctions,[2] and the interface of $In_{0.53}Ga_{0.47}As$-InP heterojunctions.[3]

von Klitzing, Dorda, and Pepper[4] first demonstrated the possibility of using the quantized Hall resistance R_H of a two-dimensional electron gas for a high-precision determination of h/e^2 or the fine-structure constant α independent of quantum electrodynamic theory. Here, R_H is defined as the ratio of the Hall emf across the device to the current through it, e is the electronic charge, h is Planck's constant. In Système Internationale (SI) units, α is given by $\alpha=(e^2/h)\mu_0 c/2$, with $\mu_0=4\pi\times 10^{-7}$ H/m and $c\equiv 2.997\,924\,58\times 10^8$ m/s.

This new application is based on the following aspect of two-dimensional electrons in strong magnetic fields applied perpendicularly to the plane of electrons at $T=0$: The Hall conductivity σ_{xy} $(=-1/R_H)$ keeps a constant value against a change in the carrier concentration or the magnetic field strength over a finite range, when the Fermi level lies in a region of localized states between ith and $(i+1)$th Landau subbands. The constant value becomes

$$\sigma_{xy}(i) = -ie^2/h\ , \tag{1}$$

when $\omega_c\tau \gg 1$ and interactions between different Landau states are absent, i.e., when the diagonal conductivity σ_{xx} vanishes. Here, i is a quantum integer, ω_c is the cyclotron frequency, τ is the relaxation time at zero magnetic field, and $\sigma_{xy}(i)$ is the ith quantized value of the Hall conductivity.

The essential part of this phenomenon was predicted by Ando, Matsumoto, and Uemura[5] in 1975, and verified experimentally by Kawaji and Wakabayashi[6] although the precision of Eq. (1) was unexpected. They[6] have shown for silicon MOSFET's that σ_{xy} attains to the "$-ie^2/h$" value even before electrons fill up the ith (lower) Landau subband and stays at the value until electrons occupy part of the $(i+1)$th (higher) Landau subband, and have pointed out that the constant (so-called plateau or step) region of σ_{xy} results from immobile carriers, i.e., immobile holes in the upper edge of the lower Landau states and immobile electrons in the lower edge of the higher Landau states, in agreement with the theoretical prediction.

The first precision measurement of R_H carried out at $T=1.8$ K with magnetic inductions $B\simeq 14$ T for silicon

 ©1986 The American Physical Society

MOSFET's[4,7] stimulated various theoretical[8–14] and experimental[15–18] studies of the quantum Hall effect. Theoretical studies have shown that the quantization of σ_{xy} is exactly in units of $(-h/e^2)^{-1}$ in the limit of a strong magnetic field, for special geometries, zero temperature, etc. However, no convincing theoretical basis has been obtained as yet to estimate uncertainties in Eq. (1) which can be finite under real experimental conditions.

Measurements of R_H values have been made by several groups with improved precision for silicon MOSFET's[7,15] ($B=14$–15 T, $T=1.4$–1.8 K) and for GaAs-$\mathrm{Al}_x\mathrm{Ga}_{1-x}\mathrm{As}$ heterojunctions[17,18] ($B=6$–9 T, $T=1.5$ K). The values of the fine-structure constant obtained from the results of these measurements and also those obtained from other methods[19,20] coincide with one another to within the experimental uncertainty of ~ 1 ppm. This fact indicates that, to within ~ 1 ppm, R_H is independent of the material of the interface where the two-dimensional electrons are trapped, as well as the magnetic field, temperature, and the concentration of electrons.

The primary limitation for obtaining the absolute value of R_H (in SI units Ω_{SI}) is the uncertainty associated with the unit of resistance. The uncertainty is $\sim \frac{1}{2}$ ppm for the Electrotechnical Laboratory unit maintained at the 1-Ω level, for instance. On the other hand, one can compare two or more well-quantized values of $R_H(i)$ associated with different plateaus which occur in a single sample and examine the accuracy of the relationship

$$\sigma_{xy}(i)/i=\sigma_{xy}(j)/j=\mathrm{const}\ , \tag{2}$$

regardless of the uncertainty associated with the unit of resistance. The result of comparisons between three kinds of plateaus, $i=4$, 8, and 12, for a silicon MOSFET sample indicates that Eq. (2) holds with a possible deviation of less than 2 parts in 10^7, which is the limit of resolution for our preliminary measurement system.[21]

Results of both the experimental and theoretical studies suggest that the quantum Hall effect can be applied to improve the determination of fundamental constants to within parts in 10^8 uncertainty. Therefore, it is required to find the conditions under which the quantization is considered to be perfect and the same experimental result is always reproduced with this accuracy.

The purpose of the present experiment is to study, at the highest limit of accuracy which can be achieved by the available experimental techniques, the following problems: (1) the accuracy of Eq. (2) under various experimental conditions, and (2) the fundamental physical limitations which determine the inherent accuracy of Eq. (1). The result for silicon MOSFET's indicates that cooling the sample down to ~ 0.5 K is important in order to approach one of the ideal conditions, $\sigma_{xx}\to 0$. This paper also describes the equipment and procedures which are essential for high-accuracy measurements at liquid-^{3}He temperatures with uncertainties of less than a few parts in 10^7, so that the present results can be reproduced by independent measurements.

In Sec. II we describe the equipment and techniques used. Some details of the ^{3}He-cryostat system used are included, since commercially available ^{3}He cryostats are usually less adequate for the purpose of precision measurement of dc voltages. In Sec. III we show experimental results and derive experimental conditions under which the same value of R_H is reproduced to within a few parts in 10^7, i.e., a criterion of a well-quantized (or "ideal" in the practical sense) Hall plateau on which the measurement of R_H will give the fundamental constant h/e^2. In Sec. IV we present the results of high-accuracy measurements which verify the relationship given by Eq. (2) and its long-term reproducibility to within the limit of experimental uncertainty.[22] Section V contains discussions of the factors contributing to the uncertainty, and also of the requirement for further improvement in resolution and linearity of voltage comparisons. In Sec. VI we summarize the conclusions.

II. EXPERIMENTAL EQUIPMENT AND PROCEDURE

A. Outline of the measurement and sample

The Hall and diagonal resistivities were measured for n-channel (100) inversion layers of silicon MOSFET's at temperatures down to ~ 0.5 K. Magnetic inductions up to 15 T were applied perpendicularly to the inversion layers. Figure 1 shows a schematic diagram of (a) the present measuring circuit and (b) the shape and probe ar-

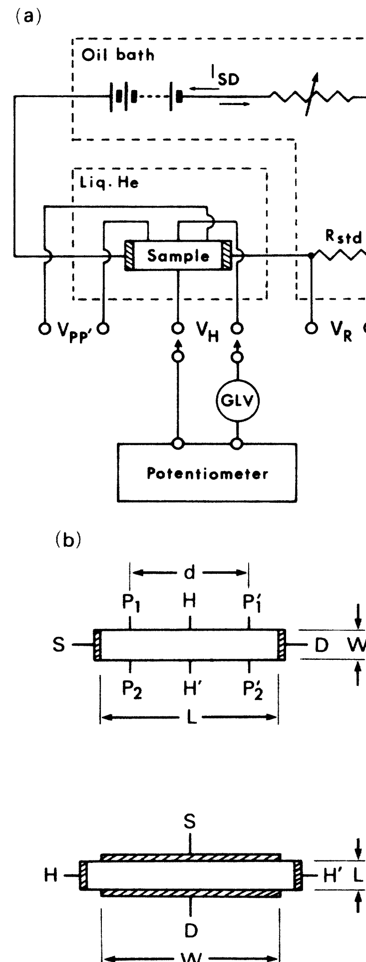

FIG. 1. Schematic diagrams of (a) the measurement circuit, and (b) shape and probe arrangement of samples.

rangement of the samples. A constant-channel (source-to-drain) current I_{SD} flows through both the sample and a reference resistor R_{std}, and R_H is measured via R_{std} in terms of the Electrotechnical Laboratory (ETL) as maintained unit of resistance Ω_{ETL}.

The quantum Hall effect is observed as a series of flat plateaus in a chart recording of the Hall emf V_H against the gate voltage V_g in a strong magnetic field. The high-accuracy measurements were made in regions of V_g over which V_H appeared to be unchanged and $V_{PP'}$, the potential drop between two points P and P' along the channel current, was sufficiently small.

The silicon MOSFET samples were obtained from the Research Center, Sony Corporation. Details of the fabrication of MOS devices and their characterization have been given by one of the authors,[23] but we include a partial repetition here. The MOSFET's are fabricated on a (100) plane of p-type silicon doped with $\sim 2\times 10^{20}$ boron atoms m^{-3}. To reduce leakage current from the outside of the gate area, a heavily-boron-doped region (channel stop) is formed around the gate area by ion implanation at 5×10^{18} boron atoms m^{-2} in dose. Figure 2(a) shows the cross-sectional view of a silicon MOSFET. A silicon chip of 1.91×1.91 mm^2, on which several MOSFET's are fabricated, is enclosed in a ceramic package of $10\times 10\times 1$ mm^3. Figure 2(b) shows the top view of the uncovered package.

The concentration of two-dimensional electrons n_s for the present samples is approximately proportional to V_g and is changed to $\sim 4\times 10^{16}$ m^{-2} by adjusting V_g up to + 50 V without affecting the reproducibility of the data.

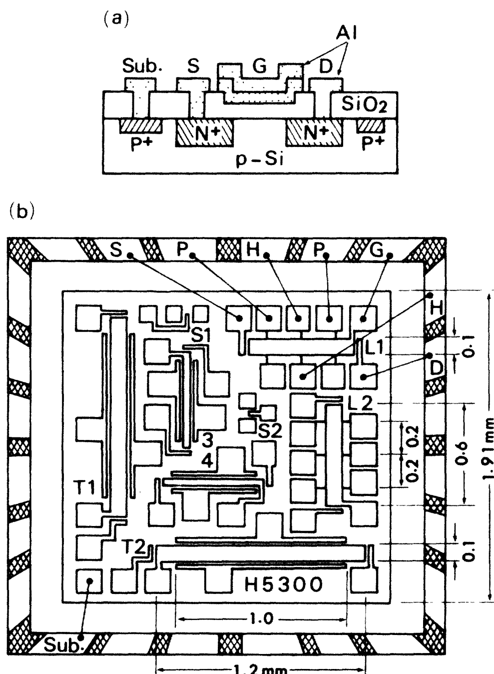

FIG. 2. Schematic diagrams of (a) cross-sectional view of a silicon MOSFET, and (b) top view of uncovered package. G, aluminum gate; S and D, source and drain electrodes; N^+, heavily doped n-type region with $> 10^{26}$ phosphorus atoms m^{-3}; P^+, heavily doped p-type region formed by ion implantation at 5×10^{18} boron atoms m^{-2} in dose; Sub, substrate electrode.

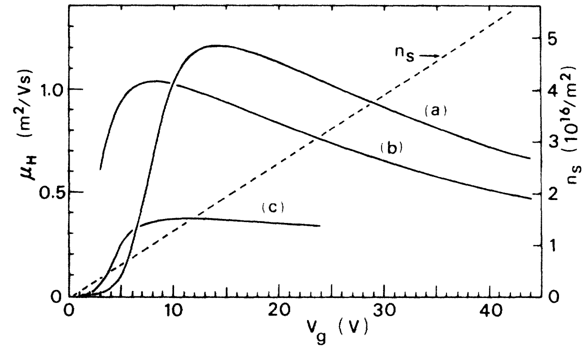

FIG. 3. μ_H (at $B\to 0$) as a function of V_g for typical samples: (a) high-mobility sample (72H53-17$T2$) at 4.2 K, (b) high-mobility sample (62H53-17$L1$) at 1.4 K, and (c) low-mobility sample (N9-8H53-02) at 1.5 K. n_s, density of 2D electrons for sample (b).

The Hall mobility μ_H also changes as a function of V_g. Figure 3 shows the Hall mobility (at the limit of $B=0$) for three typical samples, i.e., two high-mobility samples and a low-mobility sample. The value of n_s is also shown in the figure as a function of V_g for one of these high-mobility samples.

Table I lists the samples used, their oxide layer thickness δ, length L, and width W of the electron channel, and maximum Hall mobility μ_H^{max} on the μ_H-versus-V_g curves at liquid-helium temperatures.

Samples have been stored at room temperature more than three years without appreciable change in Hall and diagonal resistivities.

B. Cryogenic equipment

Commerically available ^{3}He-cryostat systems are designed primarily so as to cool samples down to ~ 0.3 K by minimizing heat leaks. For the purpose of precision dc measurements, on the other hand, minimizing thermal emf's along the lead wires is of primary importance, which is reached at the expense of the lowest temperatures to be attained. We include here details of the ^{3}He-cryostat systems constructed for the present experiment.

Three superconducting-magnet and cryostat systems were used. (a) $B=15$ T, $T=1.4$ K system: Measurements with this system were made at the Institute for Solid State Physics, University of Tokyo (ISSP). Magnetic inductions up to 15 T were generated at 4.2 K by a superconducting magnet of Intermagnetics General Corporation, or IGC (32-mm clear bore, pancake type made of stabilized Nb_3Sn tape); the samples were immersed directly in liquid helium and cooled to ~ 1.4 K. (b) $B=10.5$ T, $T=0.5$ K system: A 10.5-T IGC superconducting (SC) magnet (32-mm clear bore, solenoid type made of Ti-Nb multifilament wire) was used at temperatures below 2.2 K; the samples were immersed directly in liquid ^{3}He and cooled to ~ 0.5 K. (c) $B=12$ T, $T=0.5$ K system: A 12-T IGC SC magnet (32-mm clear bore, pancake type made of stabilized Nb_3Sn tape) was used at 4.2 K; the samples were immersed directly in liquid ^{3}He and cooled to ~ 0.5 K.

We constructed two different ^{3}He cryostats and three sample holders of the same size and design. Figure 4 il-

TABLE I. List of silicon MOSFET samples investigated.

Code	Sample	δ (nm)	L (μm)	W (μm)	μ_H^{max} (m^2/V s)
A	62H53-17-1*L*1	200	600	100	1.03
B	62H53-17-1-*L*2	200	600	100	1.03
C	62H53-17-11-*L*1	200	600	100	1.03
D	72H57-1-13	200	3200	3200	1.10
E	44-4-11-*L*	800	500	100	1.19
F	N9-7H53-22-*L*2	150	600	100	0.65
G	N9-8H53-21-*L*2	150	600	100	0.38
H	72-1H53-D1-*L*1	200	600	100	1.20
J	72-1H53-D1-*L*2	200	600	100	1.20
K	72-17H53-14-*L*1	200	600	100	1.36
L	72-17H53-15-*L*1	200	600	100	1.36
M	72-17H53-17-*L*1	200	600	100	1.36
N	72-17H53-18-*L*1	200	600	100	1.36
P	72-17H53-18-*T*1	200	100	1000	1.36
Q	72-17H53-19-*L*1	200	600	100	1.36
R	72-17H53-20-*L*1	200	600	100	1.36
S	72-17H53-D3-*L*1	200	600	100	1.36
T	72-17H53-D4-*L*1	200	600	100	1.36
U	72-18H53-01-*L*2	200	600	100	1.36

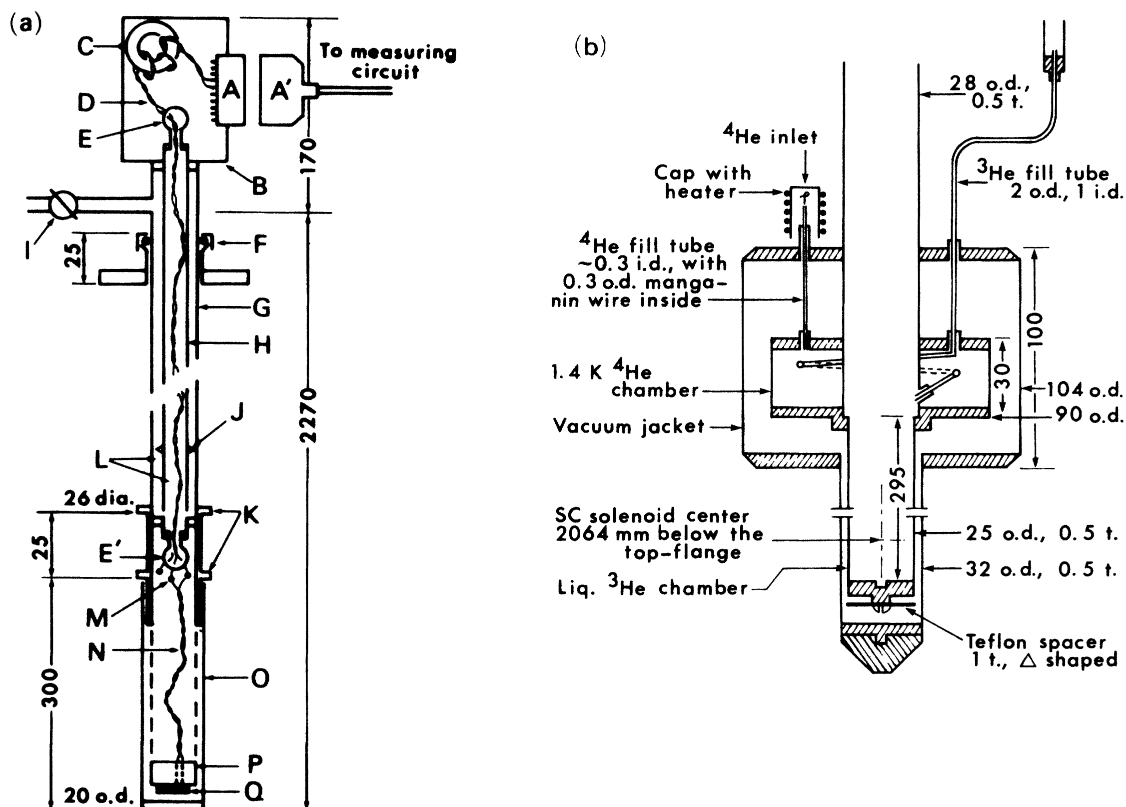

FIG. 4. Parts of the cryogenic equipment. (Not to scale. Dimensions are in mm unless otherwise indicated.) (a) Sample holder. *A*, Amphenol 57-40500 50 pin connector; *A′*, Amphenol 57-30500 50 pin connector; *B*, aluminum chassis (120×80×40); *C*, ferrite toroidal core, on which twisted pairs of copper wire are wound; *D*, twisted pairs of copper wire (Formvar-insulated, 0.16 diam., ~2500 long); *E* and *E′*, electrical feedthroughs (304 stainless-steel tubing, 6.0 o.d., 0.2 thick), sealed with a mixture of Epoxy resin and Al_2O_3 powder; *F*, sliding-seal arrangement; *G*, cupronickel 70-30 tubing (16 o.d., 0.5 thick); *H*, cupronickel 70-30 tubing (8—11 o.d., 0.5 thick); *I*, $\frac{3}{8}$-in. value for vacuum-space evacuation; *J*, Teflon spacers; *K*, radiation shields; *L*, vacuum tight space; *M*, soldered joints of copper wire and Ti-Nb wire; *N*, copper-coated Ti-Nb superconducting wire (Formvar-insulated, 0.1 diam., ~400 long); *O*, cupronickel 70-30 tubing to cover the sample and wires (20 o.d., 0.5 thick); *P*, bakelite cylinder (18.8 diam., 7 thick); *Q*, sample. (b) Liquid-^{3}He chamber. Tubings to ^{3}He and ^{4}He pumping systems are not shown for clarity. The rate of ^{4}He flow into the 1.4-K ^{4}He chamber is adjusted with a manganin wire (<0.3 diam., 1.8×10^{17} m^{-3} flow impedance factor).

lustrates a sample holder and a part of the ^{3}He cryostat for system (c). The sample holders are designed so that (1) thermal emf's along the electrical leads and their variations with time are minimized, (2) each holder can be inserted in any cryostat of the three systems, and (3) samples are easily exchanged by replacing the whole holder with another without introducing much air into the cooled cryostat. The electrical leads, which are 9 or 10 twisted pairs of copper wire (Formvar-insulated, 0.16 mm diam, ~2500 mm long), run from an Amphenol 57-40500 connector A to soldered joints M in a sample chamber O, without any joint between A and M. These leads are doubly enclosed in thin-walled cupronickel tubings, and the enclosed space L is evacuated so that the leads are in moderate thermal insulation from the liquid-helium bath. The temperature distribution along the leads is thus insensitive to the liquid level, though the evaporation rate of liquid ^{3}He increases as compared with the case where there is complete thermal exchange. The leads are connected at their lower ends M with copper-coated Nb-Ti wires N running down to the sample. The Nb-Ti wires are loosely curled so as to keep a good thermal contact via ^{3}He-gas flow to the cooled liquid ^{4}He, which is stored in the 1.4-K chamber. The heat inflow along the leads amounts to ~50 mW, nearly all of which is absorbed into the cooled liquid ^{4}He. The lower fin of the radiation shield K is placed just above the diameter gap of the two tubings of 28 mm o.d. and 25 mm o.d., at the bottom of the 1.4-K chamber. It is not necessary for the fins to mechanically touch the cooled wall. The net amount of heat flow into the ^{3}He chamber is estimated to be less than 100 μW. A lowest temperature of 0.47 K is obtained in normal use. The package of the silicon MOSFET's is attached to the bottom of bakelite cylinder P with double-sided adhesive tape. The insulation resistance of the bakelite cylinder is high enough at liquid-helium temperatures.

When the sample holders were not in use, all the probes and electrodes of the samples were short-circuited and grounded. This was needed to protect the samples from possibly charging up due to the highly insulated circuits.

It was possible to maintain temperatures around 0.5 K for more than 12 h for system (c) and more than 6 h for system (b), with a 150-l/min mechanical pump (for ^{3}He-gas evacuation through 28.6-mm-o.d. tubing) and 10 l (at STP) of ^{3}He gas.

C. Measuring equipment

1. Channel-current source and standard resistor

The current source for I_{SD} consists of eleven 1.35-V mercury batteries, a current-reversing switch, and a series of step-variable resistors with two selector switches. These switches are Fujitsu 125D rotary switches (ceramic wafers, eleven positions) in which bakelite insulation is replaced by Teflon to improve electrical insulation. They are mounted on an acrylic plate and operated via Delrin (polyacetal) rods (6 mm diam, 150 mm long) to minimize the electrical leakage and heat flow from the operator to the contact points. The channel-current source and a Yokogawa Electric Works 2781 standard 10-kΩ resistor were mounted on acrylic plates, housed together in an oil bath, and directly immersed in the oil. The oil bath was designed so as to (1) minimize the effect of changes in room temperature, (2) keep a fixed temperature distribution, and (3) shield electrostatic inductions. The oil bath is an aluminum box (360×300 mm^2 floor space, 250 mm deep, 6 mm thick) enclosed in polystyrene foam walls (30 mm thick) and an aluminum case (1 mm thick) having orifices for lead wires, thermometers, and the Delrin rods.

Temperatures in the oil bath were measured and monitored at the center of the standard 10-kΩ resistor with a mercury-in-glass thermometer (0.1 °C accuracy around 20 °C) or a standard platinum-resistance thermometer (Chino Works Ltd., 25 Ω nominal, 0.01 °C accuracy, 0.001 °C resolution, used on and after 23 March 1983), and a precision thermistor (Yellow Springs Instruments 44005, 3.76 kΩ and −166 Ω/deg at 20 °C, 0.01 °C resolution). We did not control the bath temperature, but rather let it reach its thermal-equilibrium value. Although the bath temperature changed slightly with variations in room temperature, we selected the period of time during which we could maintain an appropriate constant temperature for the measurement, which was several hours around

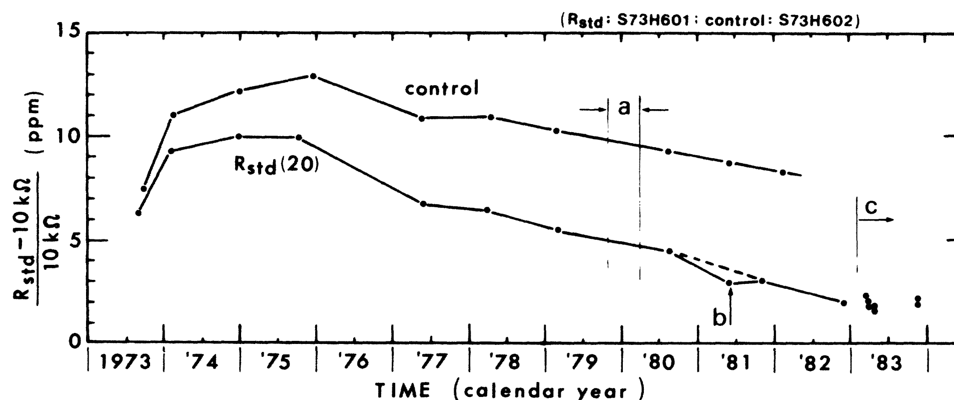

FIG. 5. Time variation of resistance values for two YEW-2781 10-kΩ resistors (after Murakami, Ref. 24). Control: the resistor which has been kept in a constant environmental condition since Feb. '80. *a*, interval during which the ETL (Tokyo) moved to Ibaraki; *b*, result of measurement made shortly after a thermal shock (from 27 to 20 °C); *c*, since Mar. '83 the operator has changed.

TABLE II. Calibration data for standard 10-kΩ resistor [YEW 2781 10-kΩ resistor (S73H601)].

Date of calibration	t_{cal} (°C)	$R_{std}(t_{cal})$ (Ω_{ETL})	$R_{std}(20)$ (Ω_{ETL})
25 Aug. '80	20.00	10000.0451	10000.0451
2 June '81	20.00	10000.0300	10000.0300
30 Oct. '81	23.38	10000.0690	10000.0306
29 Nov. '82	17.95	9999.9962	10000.0196
11 Mar. '83	18.1	10000.0020	10000.0240
11 Mar. '83	18.1	10000.0021	10000.0241
16 Mar. '83	18.1	9999.9990	10000.0210
16 Mar. '83	18.1	9999.9975	10000.0195
20 Apr. '83	18.1	9999.9946	10000.0166
26 Apr. '83	17.8	9999.9933	10000.0188
15 Nov. '83	19.989	10000.0200	10000.0200
16 Nov. '83	20.006	10000.0231	10000.0231

midnight excluding June to September, the period of high relative humidity. As a result, the oil-bath temperature was kept constant to within ±0.03 °C for the duration of the measurement.

The value of $R_{std}(t)$ for the standard 10-kΩ resistor used was given as

$$R_{std}(t)-R_{std}(20)=10^{-2}\times[1.151(t-20)-0.004(t-20)^2]\Omega_{ETL}\ , \quad (3)$$

based on measurements performed at temperatures between 17 and 25 °C (in February 1975), where t is the oil-bath temperature in °C and the value of $R_{std}(20)$ varies with time as shown in Fig. 5.[24] Table II lists recent calibration data of the standard 10-kΩ resistor together with the date and temperature t_{cal} at which the calibrations were made.

2. *Circuits and leads*

A simplified circuit diagram of the emf-measuring circuit and that of the gate-voltage-supply circuit are shown in Figs. 6 and 7, respectively. These circuits (exclusive of the channel-current source, standard 10-kΩ resistor, and other reference resistors which were contained in the oil bath) were mounted on acrylic plates and housed individually in two aluminum boxes. Switches used in these circuits were operated from the outside via Delrin rods. The purpose of these aluminum boxes was to shield electrostatic inductions and also to maintain an environment of

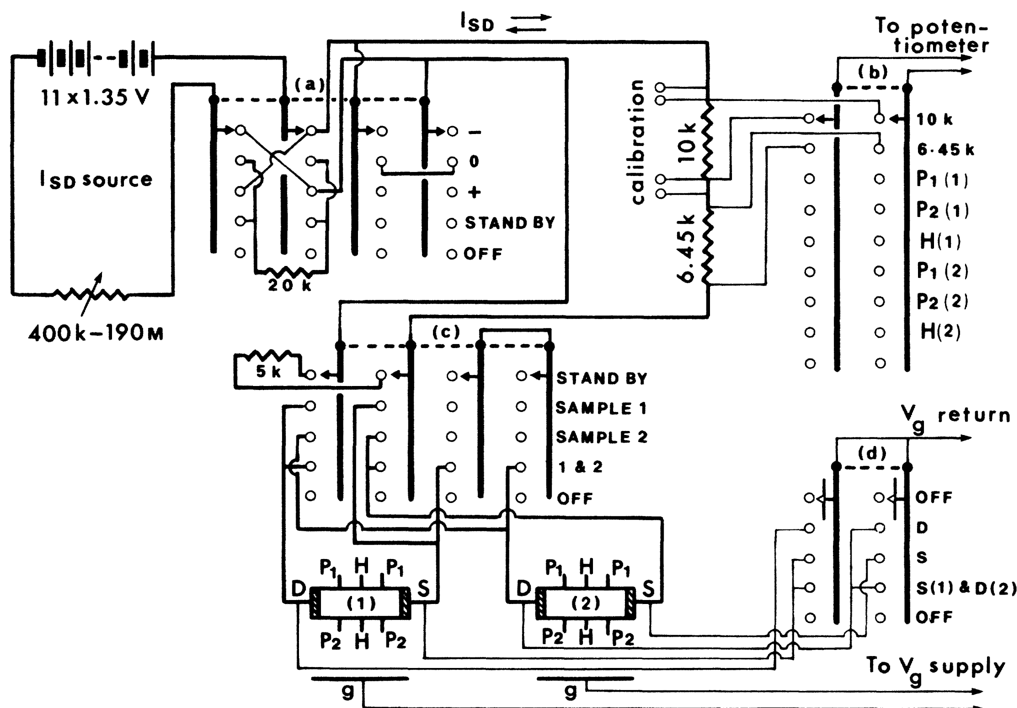

FIG. 6. Simplified circuit diagram of the emf-measuring circuit. Values of resistances are in Ω; switch blades noted by triangles-with-arms function without simultaneously breaking both circuits. (a) I_{SD} reversing switch; (b) emf selector switch; (c) sample selector switch; (d) V_g reference electrode selector switch.

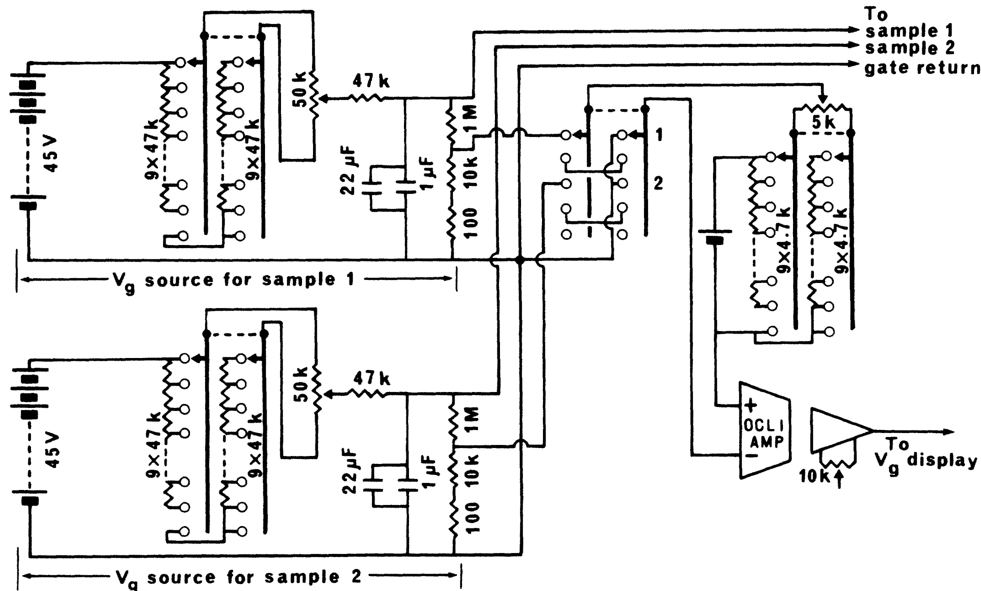

FIG. 7. Simplified circuit diagram of the gate-voltage-supply circuit. Values of resistance are in Ω. OCLI AMP, optically coupled linear amplifier (Burr-Brown 3652 JG). 47 kΩ resistor, 22 μF tantalum electrolytic capacitor, and 1 μF plastic film capacitor make a low-pass filter which prevents an abrupt change of V_g.

fixed temperature distribution for the circuits contained. As the emf selector switch, we used a Guildline Instruments Model 9145A five-position push-button switch which was selected from various switches, including those of the same model, because it had the highest insulation resistance. The leakage resistances were examined between neighboring switches, between terminals of an individual switch (for "off" position), and between an individual switch and the guard shield; the values were $\sim 10^{13}$ Ω for each position.

The leads outside the cryostat, i.e., from the circuits to the sample holder were made of 9 or 10 tightly twisted pairs of copper wire (Formvar-insulated, 0.65 mm diam, 5–6 m long), each wire being enclosed in heat-resisting-polyethylene tubing (1.0 mm i.d., 1.5 mm o.d.) to keep a high insulation resistance of 10^{14}–10^{15} Ω between the paired wires. These pairs were doubly enclosed together in copper braid tubings spaced coaxially with polyvinyl chloride (PVC) tubing (15 mm, i.d., 17 mm o.d), and wrapped in PVC tape to insulate the outer copper braid tubing from ground and prevent undesirable ground loops. These leads were connected to the circuits with acrylic binding posts. The other ends of the leads were soldered to an Amphenol 57-30500 connector, A' in Fig. 4(a), which had an insulation resistance of greater than 10^{13} Ω between neighboring pins and also between an individual pin and the outer covering.

All the leads and wiring in the measuring circuits were made using tightly twisted pairs of copper wire taken from a single spool to minimize magnetic pick-up and thermal emf's. The whole circuit was enclosed in aluminum boxes and copper braid tubings, which comprise an overall electrostatic shield grounded at one point. The leakage resistance between the whole circuit and the electrostatic shield was greater than 10^{12} Ω.

It has been found that the cryostat system should be isolated from the floor, the Dewar-supporting structure, the pumping system, etc., in order to minimize external noise introduced via ground loop. This procedure is especially effective for a large system.

D. Experimental procedure

The Hall emf V_H and the potential drop across the standard 10-kΩ resistor, V_R, were individually balanced against a Guildline Instruments Model 9930 direct-current-comparator (GI-9930 DCC) potentiometer to obtain a null reading. The null was obtained using (1) a GI-9460A photocell galvanometer amplifier and a strip-chart recorder, or (2) a battery-operated Leeds and Northrup Model 9829 (LN-9829) linear amplifier, a strip-chart recorder, and a Takeda Riken TR-6501 digital volt-ohm-ratio (TR-6501 DVOR) meter. The TR-6501 DVOR meter displays the average of 20 successive readings which are taken once a second from the output voltage of the LN-9829 linear amplifier; the output voltage is monitored continuously by the strip-chart recorder to examine whether the noise, which is superimposed on the "null" signal, is random. We refer to this average value as a "reading." The current and voltage resolution are $(5–15)\times 10^{-13}$ A and $(3–10)\times 10^{-9}$ V, respectively.

For the measurement of V_H and V_R, two sets of twelve readings were taken with opposite directions of I_{SD}, in the order as shown in Table III, so as to eliminate the thermal emf's, their uniform drifts, and a long-term drift of the channel current. It requires 25–30 min to complete the series of twelve readings, from which two data points for R_H are obtained because once a switch is operated, a time interval of 2–3 min is necessary for the channel current and/or the emf's to reach their respective equilibrium value. On the other hand, longer intervals cause an increase of nonlinearity in the drift of the thermal emf's

TABLE III. Example of a typical run at $B=12$ T, $T=0.47$ K, and $I_{SD}\simeq10$ μA. Date, 31 Jan '83; sample, R. H(1), $10k$, and $P_1(1)$ denote positions of emf selector switch (b) in Fig. 6.

No.	Position of emf selector switch	Polarity of I_{SD}	emf Dial reading (10 nV)	emf Deviation from balance (600 nV)	Time and [V_g (V)]
					22:17.0 [12.051]
11	H(1)	−	−6 336 570	+0.01	47.0
12	$10k$	−	−9 819 300	+0.04	49.0
1	H(1)	−	−6 336 570	−0.01	51.0
2	$10k$	−	−9 819 300	−0.07	53.0
3	H(1)	−	−6 336 570	−0.03	55.0
4	H(1)	+	+6 336 600	−0.07	57.0
5	$10k$	+	+9 819 330	+0.04	59.0
6	H(1)	+	+6 336 600	−0.00	23:01.0
7	$10k$	+	+9 819 330	+0.06	03.0
8	H(1)	+	+6 336 600	−0.01	05.0
9	$10k$	+	+9 819 330	+0.07	07.0
10	$10k$	−	−9 819 300	−0.03	09.0
11	H(1)	−	−6 336 570	−0.00	11.0
12	$10k$	−	−9 819 300	−0.02	13.0
0	H(1)	−	−6 336 570	−0.01	15.0
0	$10k$	−	−9 819 300	−0.08	17.0
1	$P_1(1)$	−	0	+0.14	19.0
2	$P_1(1)$	+	0	+0.18	21.0
0	$P_1(1)$	−	0	+0.14	23.0
0	$P_1(1)$	+	0	+0.21	25.0
					23:27.0 [12.047]

which is difficult to eliminate. The measurement of V_{SD} or $V_{PP'}$ is essentially the same as that of V_H.

The gate voltage is applied between the gate electrode and one of the source-drain electrodes, S or D in Fig. 2(a). The reference electrode, S or D, can be switched over from one to the other using a selector switch [(d) in Fig. 6] at every polarity reversal of I_{SD} so as to keep the average value of V_g, relative to the two-dimensional-electron system, unchanged against the change of the current direction (assuming a uniform electric field distribution in the channel). This procedure was applied when the Hall plateau (or the region where $V_{PP'}\simeq0$), which appeared in a chart recording of the V_H- (or $V_{PP'}$-) versus-V_g trace, was not sufficiently wide compared with V_{SD} ($\gtrsim V_H$): data given in Fig. 9 (exclusive of data obtained using $I_{SD}<10$ μA), Fig. 11 (exclusive of one data point), Figs. 12, 14, 15, and 17, and 16–20 Oct. 1981 data listed in Tables V and VI.

We define R_H, R_{SD}, and $R_{PP'}$ in this paper as

$$R_Z \equiv R_{\rm std}(k/m)\sum^m V_Z \Big/ \sum^k V_R \ , \qquad (4)$$

where subscript Z stands for H, SD, and PP'; $R_{\rm std}$ is the resistance value obtained from a reference resistor such as given by Eq. (3); $\sum^k$ (or $\sum^m$) denotes the sum over k (or m) readings of the corresponding voltage taken from a set of $(k+m)$ readings which should give a single data point.

The components of the resistivity tensor, ρ_{xx} and ρ_{xy}, and those of the conductivity tensor, σ_{xx} and σ_{xy}, are obtained from measurements as follows:

$$R_H=\rho_{xy}=-\sigma_{xy}/(\sigma_{xx}^2+\sigma_{xy}^2)\simeq-1/\sigma_{xy}$$

and

$$R_{PP'}=(d/W)\rho_{xx}=(d/W)\sigma_{xx}/(\sigma_{xx}^2+\sigma_{xy}^2)\ .$$

Here, d is the distance between P and P', W the channel width, and $d/W=4$ for the samples used.

III. EXPERIMENTS TO FIND NECESSARY CONDITIONS FOR h/e^2 DETERMINATION

A. R_H-versus-V_g and $R_{PP'}$-versus-V_g curves for various values of μ_H

Figure 8 shows the Hall resistance R_H and the normal resistance $R_{PP'}$ plotted against V_g in the regions where $i=4$ plateaus occur at $B\simeq15$ T and $T=1.4$ K for three typical samples having (a) high, (b) intermediate, and (c) low Hall mobilities: the values of Hall mobility $\mu_H(V_g)$ at $B\rightarrow0$ and $T=1.4$ K are 1.36, $\sim$0.7, and 0.38 m^2/V s, respectively, when the V_g's are in the regions of their respective $i=4$ plateaus.

For the high-mobility sample the plateau is flat to

within ~ 1 mΩ (one-standard-deviation uncertainty for eight data points) in the region of V_g between 14.97 and 15.23 V in which $R_{PP'} < 40$ mΩ. Here, the minimum of $R_{PP'}$ occurs at $V_g = 15.05$ V and the minimum value is $R_{PP'}^{\min} = 3$ mΩ, or $\rho_{xx}^{\min} = 0.8$ mΩ.

For the low and intermediate-μ_H samples the Hall plateaus look as wide and as flat as those of the high-μ_H sample, whereas (1) the gate voltage at which ρ_{xx} drops to the minimum value does not coincide with that at the center of the corresponding Hall plateau, probably because of inhomogeneities in the concentration of two-dimensional electrons resulting from a potential fluctuation near the interface, (2) the value of $\rho_{xx}^{\min}$ for the low-μ_H sample is 2–3 orders of magnitude larger than that for the high-μ_H sample, (3) for the low-μ_H sample the value of R_H (at the plateau region) is lower by 2.1 ± 0.5 ppm, compared with the high-μ_H sample, and (4) for the intermediate-μ_H sample both $\rho_{xx}^{\min}$ and R_H values are in between those for the high- and low-μ_H samples, and double minima are observed in the R_{SD}-versus-V_g curve and the $R_{PP'}$-versus-V_g curve for $I_{SD} < 2.5$ μA, which are also attributed to inhomogeneities in the two-dimensional system.

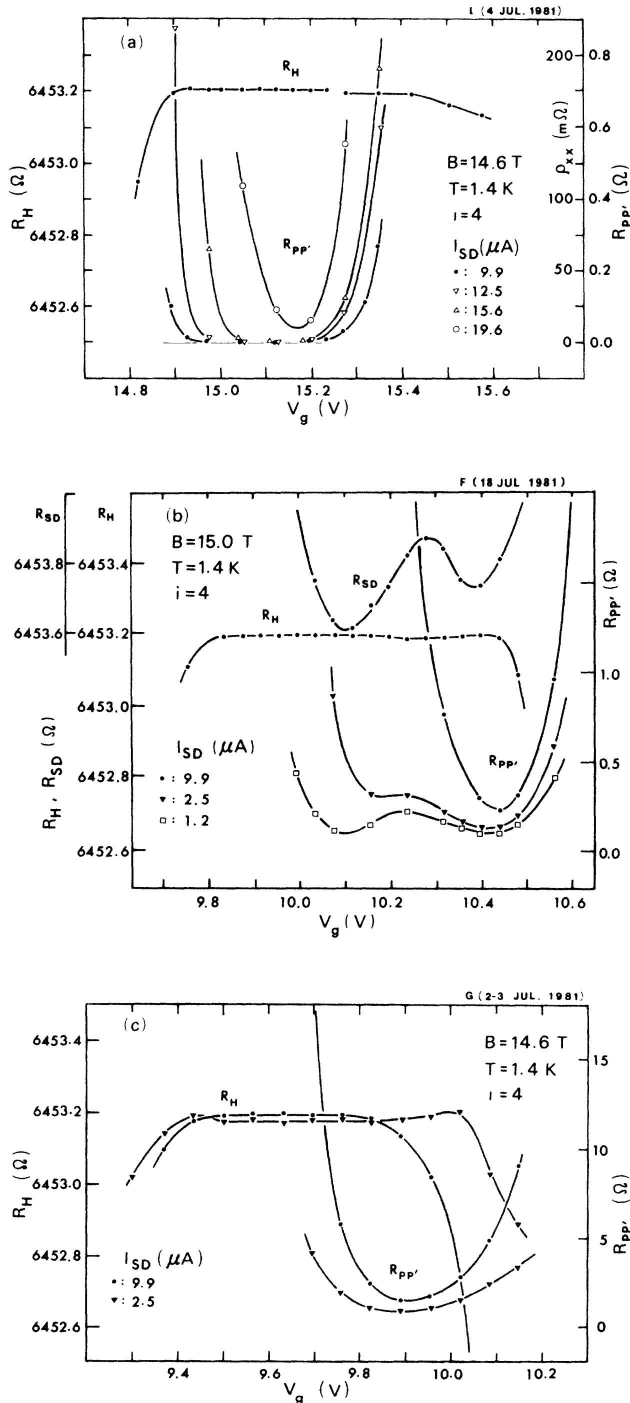

FIG. 8. R_H and $R_{PP'}$ plotted against V_g for typical samples. (a) High-mobility sample L, (b) intermediate-mobility sample F, and (c) low-mobility sample G.

B. ρ_{xx} as functions of I_{SD}, $\mu_H(V_g)$, and T

Figure 9 shows $\rho_{xx}^{\min}$ as a function of I_{SD} at $T = 1.4$ K and $B = 14.6$ T, for various values of $\mu_H(V_g)$. In the figure, $\rho_{xx}^{\min}$ is also plotted against $\mu_H(V_g)$ for $I_{SD} \simeq 10$ μA. This result indicates that $\rho_{xx}^{\min}$ increases with I_{SD} and is non-Ohmic even at the lowest values of I_{SD}, and it also increases as $\mu_H(V_g)$ is lowered.

Figure 10 shows ρ_{xx}-versus-V_g curves obtained at $T = 1.4$ and ~ 0.5 K using $B = 10.5$ or 14.6 T for V_g's in the vicinity of the $i = 4$ and 8 plateaus. The three samples used have the same characteristics. It is seen by comparing these curves that $\rho_{xx}^{\min}$ decreases as T is lowered and/or B is increased. According to the empirical criterion to be given in the following subsection, the quantization is regarded as perfect when the values of ρ_{xx} are less than 10 mΩ for $i = 4$, 5 mΩ for $i = 8$, and 3 mΩ for $i = 12$ (for the present level of accuracy). The result shown in Fig. 10 indicates that samples should be cooled down to ~ 0.5 K to use $i = 8$ or higher plateaus for the test of Eq. (2).

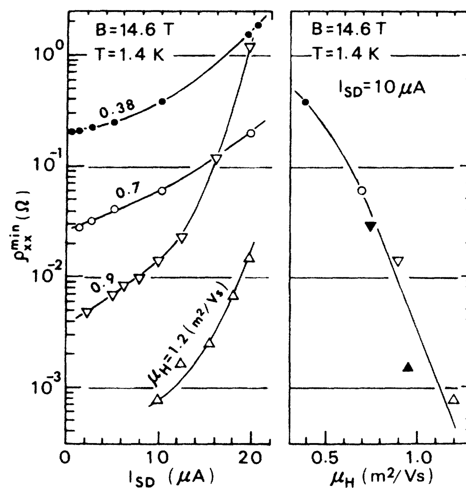

FIG. 9. $\rho_{xx}^{\min}$ as functions of I_{SD} and μ_H. Symbols (from the right top to right bottom): G, $i = 4$; F, $i = 4$; B, $i = 8$; L, $i = 8$; B, $i = 4$; L, $i = 4$.

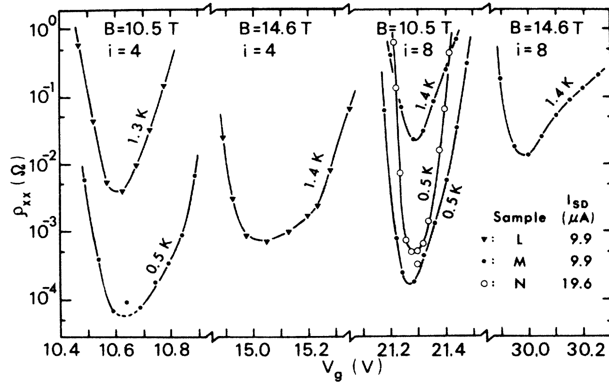

FIG. 10. ρ_{xx}-vs-V_g curves obtained under different experimental conditions.

C. ρ_{xy} as a function of ρ_{xx}

When ρ_{xx} (or σ_{xx}) is not sufficiently small, the quantization of σ_{xy} is considered to be incomplete; the value of the corresponding ρ_{xy} deviates from a constant value which should be equal to an integral fraction of h/e^2 under ideal conditions as the theories assume. Figure 11 shows the observed relative deviation

$$\Delta\rho_{xy}(i)/\rho_{xy}(i) \equiv [\rho_{xy}(i) - \rho_{xy}^0(i)]/\rho_{xy}(i)$$

plotted against various finite values of $\rho_{xx}^{\min}/\rho_{xy}(i)$. The incomplete quantization was realized by increasing T from 0.5 to 1.6 K and/or changing I_{SD} from 0.6 to 20 μA. Here, measurements of $\rho_{xy}(i)$ were made at the values of V_g where $\rho_{xx} = \rho_{xx}^{\min}$,[25] and as $\rho_{xy}^0(i)$ we took the value of $(4/i)\rho_{xy}(4)$ obtained under the condition of lowest excitations, $\rho_{xx} \ll 10$ mΩ, within a few days of the $\rho_{xy}(i)$ measurements. Since the Hall plateaus were narrow ($\lesssim V_{SD}$) in most cases, the reference point of the V_g supply was adjusted as described in Sec. II D at every polarity reversal of I_{SD}. For the data point located at $\rho_{xx}^{\min}/\rho_{xy} = 6\times10^{-5}$, which came from the value of R_H on the right-hand side edge of the $i=4$ plateau in Fig. 8(c), the above procedure was not applied, but some correction was made by comparing pairs of V_H-versus-V_g curves for $+I_{SD}$ and $-I_{SD}$; the error bar attached to this point denotes the range of the data change due to possible temperature variations in V_H in the edge region. The parameters are $\mu_H^{\max}$ (at $B\to0$, $T=1.4$ K), B, and i. In spite of the fact that measurements were made for many different parameters, data points in the figure gather around a line which is given by

$$\Delta\rho_{xy}(i)/\rho_{xy}(i) = -s\rho_{xx}^{\min}(i)/\rho_{xy}(i) \quad \text{where } s \lesssim 0.15 . \tag{5}$$

This result is in contrast to that derived by Laughlin,[11] which predicts the quadratic dependence of $\Delta\rho_{xy}$ on ρ_{xx} as indicated by a solid line in the figure. This is based on a finite value of σ_{xx} which is caused by the thermal excitation of carriers to the mobility edge and a simple symmetric landau-subband picture where electron-hole symmetry holds exactly.

A finite σ_{xx} can be also caused by the variable-range-hopping conduction of electrons and holes in the localized states at finite temperatures. However, the Hall mobility of the variable-range-hopping conduction $|\sigma_{xy}/\sigma_{xx}|_{\rm VRhop}$ for the present samples is estimated at $\lesssim 10^{-2}$ from the temperature dependence of $\rho_{xx}^{\min}$ around $T=1$ K and an expression given by Wysokinski and Brenig.[26] This value is an order of magnitude too small to explain that $s\simeq10^{-1}$ in Eq. (5).

Dashed lines in Fig. 11 represent the deviation of ρ_{xy} due to the shorting effect of the source and drain electrodes calculated after Lippmann and Kuhrt[27] for various values of the aspect ratio L/W.

The value of $\rho_{xx}^{\min}$ is more sensitive than ρ_{xy} to the inhomogeneity of the electron distribution in the channel, as can be seen from the difference of geometrical conditions in the measurements of ρ_{xx} and ρ_{xy}. In the figure, s varies between 0.15 and ~0 for high-μ_H samples; $s\simeq0.06$ for a low-μ_H sample. Thus, s looks independent of μ_H and $s\lesssim0.15$. However, the small value of $s\simeq0$ results from a highly inhomogeneous distribution of two-dimensional (2D) electrons, as seen in Fig. 15 below. Therefore, it could be concluded that $s\simeq0.15$ for the homogeneous electron channel with the present size and probe arrangement.

Cage *et al.*[28] have shown that the linear relation $\Delta\rho_{xy} = -s\rho_{xx}^{\min}$ holds for GaAs-Al$_x$Ga$_{1-x}$As heterojunctions to at least the 0.01-ppm level of precision, and the proportionality factor s ranges from 0.507 to 0.015 depending on the sample and conditions under which the measurements have been carried out. In this case, it is considered that the sample of $s\simeq0.5$ is the most promising for the measurements with the highest accuracy.

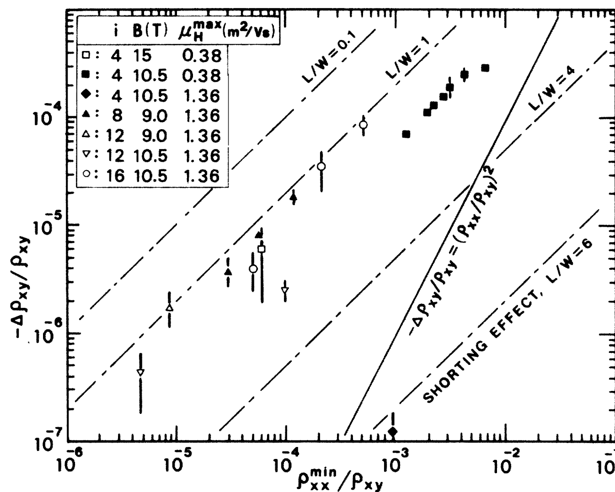

FIG. 11. Deviation of $\rho_{xy}(i)$ from "h/ie^2" for finite values of $\rho_{xx}^{\min}$. Solid line, effect of thermal excitation of carriers (after Laughlin, Ref. 11); dashed lines, effect of sample geometry for the samples with $L/W=6$, 4, 1, and 0.1, and with the Hall electrodes at $L/2$ points along each side of the channel (after Lippmann and Kuhrt, Ref. 27). Note that $-\Delta\rho_{xy}/\rho_{xy} \simeq \Delta\sigma_{xy}/\sigma_{xy}$ and $\rho_{xx}^{\min}/\rho_{xy} \simeq -\sigma_{xx}^{\min}/\sigma_{xy}$ when $\sigma_{xx} \ll |\sigma_{xy}|$, as in the present case.

D. Effect of geometrical configuration and resistance at electrodes

We made a direct comparison in the $R_H(4)$ values between a "short" sample ($L/W=0.1$) and a "long" sample ($L/W=6.0$). These samples were fabricated on the same substrate as seen in Fig. 2(b), and connected in series so that the same current passed through these two samples and the standard 10-kΩ resistor. The measurements were made at $T=1.32$ and 0.47 K with $B=10.5$ T and $I_{SD}=9.78$ μA. The gate voltage applied to the "long" sample was kept at $V_g=10.620$ V, the center of its $i=4$ plateau, and the gate voltage applied to the "short" sample $V_g^{(T1)}$ was changed from 10.64 to 10.80 V, the region of its $i=4$ plateau. Figure 12 shows the difference in the Hall resistance between "long" and "short" samples $R_H^{(L1)}-R_H^{(T1)}$ plotted against $V_g^{(T1)}$. The difference decreases as the temperature is lowered, i.e., for the samples shown in the figure the value of $R_H^{(T1)}$ is smaller than that of $R_H^{(L1)}$ by (90±38) ppm at 1.32 K and (0.6±0.2) ppm at 0.47 K. The magnitude of these differences may be explained from the geometrical effect of the "short" sample, though only qualitatively (since the sample has no probes for the measurement of ρ_{xx}).

The difference between R_{SD} and R_H is considered to give the contact resistance at the source-drain electrodes when $\rho_{xx}=0$ over the whole area of the channel. In Fig. 12, $R_{SD}-R_H$ for a "short" sample is also plotted against V_g. In this case and in the case of a "wide" sample ($W=L=3200$ μm), no difference between R_{SD} and R_H values is found to within ~0.2 ppm. On the other hand, for "long" samples the difference is $\gtrsim 0.1$ Ω over the $i=4$ plateau region at $T=1.3$ K, $B=10.5$ T, and $I_{SD}\simeq 10$ μA, as shown in Fig. 13. Table IV summarizes the result,

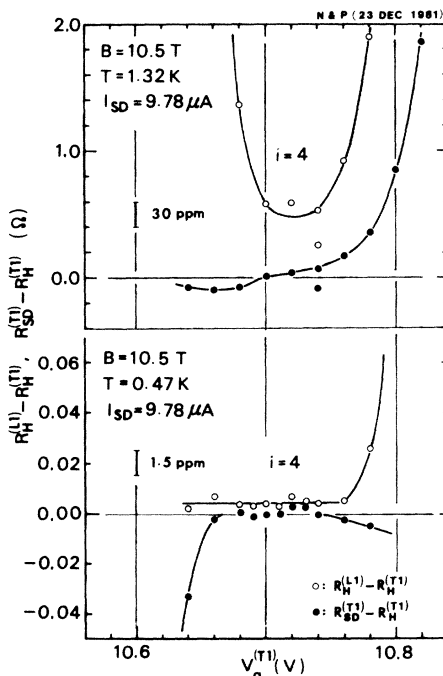

FIG. 12. Difference in R_H between "long" and "short" samples, and resistance at electrodes for the "short" sample. Samples: N (long) and P (short).

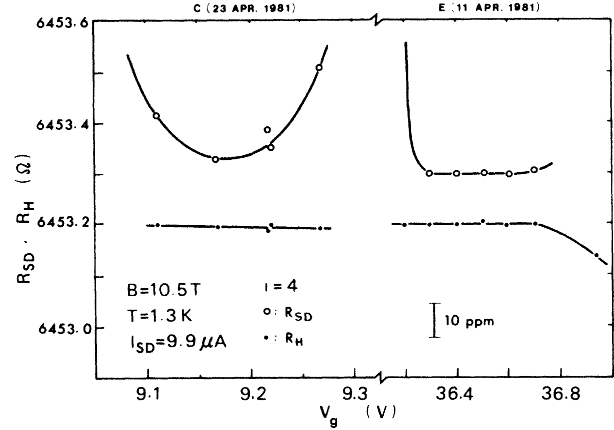

FIG. 13. R_{SD} and R_H for two "long" samples. Samples: C (left-hand side) and E.

where $\langle R_{SD}-R_H\rangle$ denotes the average of several data points obtained in the $i=4$ plateau region with $I_{SD}\simeq 10$ μA, and the error is one-standard-deviation random uncertainty. Although the value of $R_{SD}-R_H$ for the "long" samples is ~0.1 Ω per a pair of electrodes, it indeed can be far greater than $0.1\times 100/W$ (W in μm) for samples with $W<100$ μm, because the effect of dissipative regions (described in the next subsection below) is serious for relatively narrow channels.

E. Effect of electrical noise and lifetime of samples

It is important for the quantum-Hall-effect experiment to minimize noise in the measuring circuit. The main sources of noise in the present measurement system are the amplifier and external electromagnetic disturbances such as that caused by electrical machinery and a quench event of the superconducting magnet.

The following experimental results show that the effect of noise or an abrupt change in electric field distribution in the sample alters the appearances of ρ_{xx}-versus-V_g and ρ_{xy}-versus-V_g curves, especially in the regions of V_g where Hall plateaus occur.

Figure 14 shows a change of ρ_{xx}-versus-V_g curve after a quench event of the superconducting magnet from 10.5 T to zero, and the recovery from the change after being annealed over 40 h at room temperature. After the quench event, the gate voltage V_g^{min} at which ρ_{xx} falls to the minimum value has shifted from 10.63 to 10.93 V for $i=4$, and from 21.30 to 21.60 V for $i=8$, as if the threshold gate voltage has increased by ~0.3 V. The width of

TABLE IV. Comparison of $R_{SD}-R_H$ values for various samples.

Sample code	B (T)	T (K)	$\langle R_{SD}-R_H\rangle$ (Ω)
D (wide)	14.7	1.4	−0.0010±0.0017
E (long)	10.5	1.31	+0.1002±0.0035
C (long)	10.5	1.34	+0.13
P (short)	10.5	1.32	+0.0133±0.0622
P (short)	10.5	0.47	+0.0009±0.0016

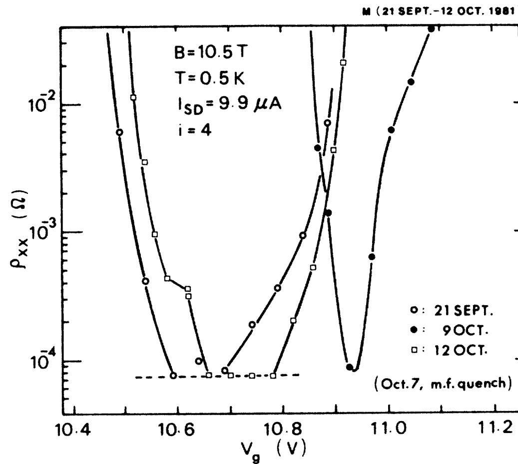

FIG. 14. Change of ρ_{xx}-vs-V_g curve after a quench event of superconducting magnet and recovery of the original character after annealing at room temperature. Sample: M.

ρ_{xx}-versus-V_g curves becomes narrower, e.g., the range of V_g in which $\rho_{xx} < 10$ mΩ decreases from 0.42 to 0.16 V for $i=4$, and the range in which $\rho_{xx} < 5$ mΩ from 0.19 to 0.08 V for $i=8$. The sample can recover its original character by being kept at room temperature, with all the electrodes shortcircuited, for 2 to 100 days depending on the strength of the electric field noise. However, the change (degradation) seems to persist if such an event and the annealing cycle is repeated more than several times for a sample.

Figure 15 shows R_H and $R_{PP'}$ as functions of V_g around $i=4$ and 12 plateaus obtained at $T=0.5$ K, $B=10.5$ T, and $I_{SD} \simeq 20$ μA. For the measurement of Dec. 19 on the $i=4$ plateau, it is seen that $\rho_{xx} \gtrsim 6$ Ω probably because of some electrical shocks prior to the measurement. The value of $R_H(4)$ deviates little from that obtained under the vanishing ρ_{xx} condition, $\rho_{xx} < 10$ mΩ: $\Delta\rho_{xy}/\rho_{xy} = -(1.1 \pm 0.8) \times 10^{-7}$ while $\rho_{xx}^{\min}/\rho_{xy} \simeq 10^{-3}$, i.e., this result corresponds to $s \simeq 0$ in the empirical relation (5). After a few days annealing at room temperature, the

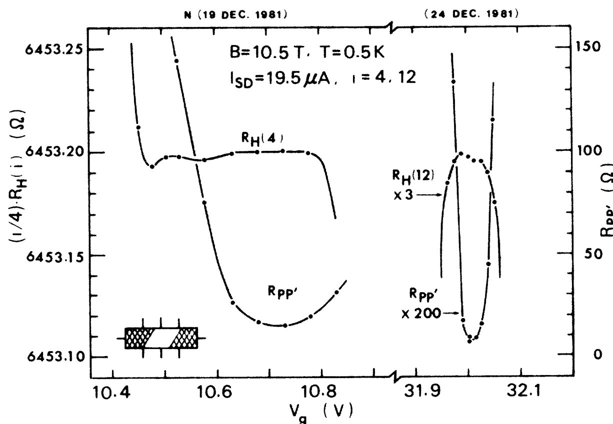

FIG. 15. R_H and $R_{PP'}$ as functions of V_g. The inset in the lower corner indicates a possible distribution of dissipative regions (hatched areas) in the channel. Sample: N.

sample recovered the small ρ_{xx} values in the plateau regions, as seen from the data of Dec. 24 for $i=12$ (in Fig. 15) and $i=8$ (open circles in Fig. 10).

These facts, as shown in Figs. 14 and 15, are understood on the assumption of an inhomogeneous-dissipative-region model proposed by Cage *et al.*[29] Under the condition of almost perfect quantization, Joule heat $V_{SD}I_{SD}$ is generated at two thin dissipative areas of $\sim W \times 2dL$ in the vicinity of the source-drain electrodes where the field strength is greatest.[30] Here, dL is $\sim \frac{1}{3}$ μm, if the electrons in these dissipative regions are accelerated up to the velocity of longitudinal lattice waves and lose their energy by emitting acoustic phonons. It has been verified experimentally that it is difficult for electron heating to occur when $\rho_{xx} \simeq 0$ holds in most of the channel.[21,30,31] However, in these dissipative regions, electric field noise would help induce hot electrons which can be injected, via direct tunneling, into localized states in the SiO_2 layer close to the SiO_2-Si interface.[32] This is inferred from the apparent shift of the threshold gate voltage and the long-detrapping-time constant of the order of a few days. These trapped electron states produce a nonuniform electric field in the inversion layer, and cause an inhomogeneous distribution of 2D electrons, or inhomogeneous dissipative regions. These regions would grow with time in the presence of electrical noise and source-drain fields, starting from the points of highest electric field (e.g., two diagonal corners in the channel) toward the center. The inset in Fig. 15 illustrates schematically a possible distribution of dissipative regions (hatched areas) in the sample. It is impossible in this case to evaluate the effect of shorting on the value of R_H merely from the geometrical configuration, W/L.

Figure 16 compares two recorder traces which display V_H-versus-V_g and $V_{PP'}$-versus-V_g curves for the $i=4$ plateau of a sample before and after the sample is exposed to electric field noise at low temperatures. These curves were obtained at $T=0.5$ K, $B=10.5$ T, and $I_{SD} \simeq 10$ μA. In the case of Fig. 16(a), $V_{PP'} < 30$ nV and the plateaus for both $+I_{SD}$ and $-I_{SD}$ are flat in the range of V_g between 10.70 and 10.85 V. In this range the dissipationless area is supposed to extend over the full length of the channel as the inset shows. In the case of Fig. 16(b), which was obtained after an interval of two weeks during which the sample was kept at liquid-helium temperatures, $V_{PP'} \simeq 0$ holds in the range of V_g between 11.05 and 11.20 V, i.e., the plateau region has shifted to higher gate voltages by ~ 0.3 V, and the V_H-versus-V_g curves are deformed. The deformation results from a V_g-dependent change in I_{SD}, as verified by comparing the V_H-versus-V_g curves with the V_R-versus-V_g curves which display the change in I_{SD} as a function of V_g. Here, V_R is the voltage drop across a 6.45-kΩ reference resistor which is in series with the sample. The values of R_H/R_R for the above [(a) and (b)] agree to within a few parts in 10^7. This fact suggests that the dissipative regions extend across the full width of the channel and cause an appreciable change in I_{SD} (~ 50 ppm in the range of V_g where $R_{PP'} \simeq 0$) but not large enough to include any of the potential probes. In this case, the aspect ratio (in effect) is considered to be at least $d/W=4$, and the value of R_H is not affected by the

corner degradation, i.e., the V_H step would be flat for constant I_{SD}.

The lifetime of samples depends on the conditions under which the measurements have been made, and also on the shape of the sample: measurements at $I_{SD} > 15$ μA and/or $V_g > 40$ V shorten the lifetime of the sample, though I_{SD} can be increased safely to 20 μA for "long" samples of highest Hall mobilities when electrical noise is sufficiently low. A persistent change in sample character was found to occur after ~200 h use for "long" samples and ~20 h use for "short" samples for measurements with $I_{SD} \simeq 10$ μA and $V_g = 10$–20 V. Since localized donor states in the SiO_2 layer only slowly release the trapped electrons at low temperatures, samples require some annealing intervals during the course of experiments.

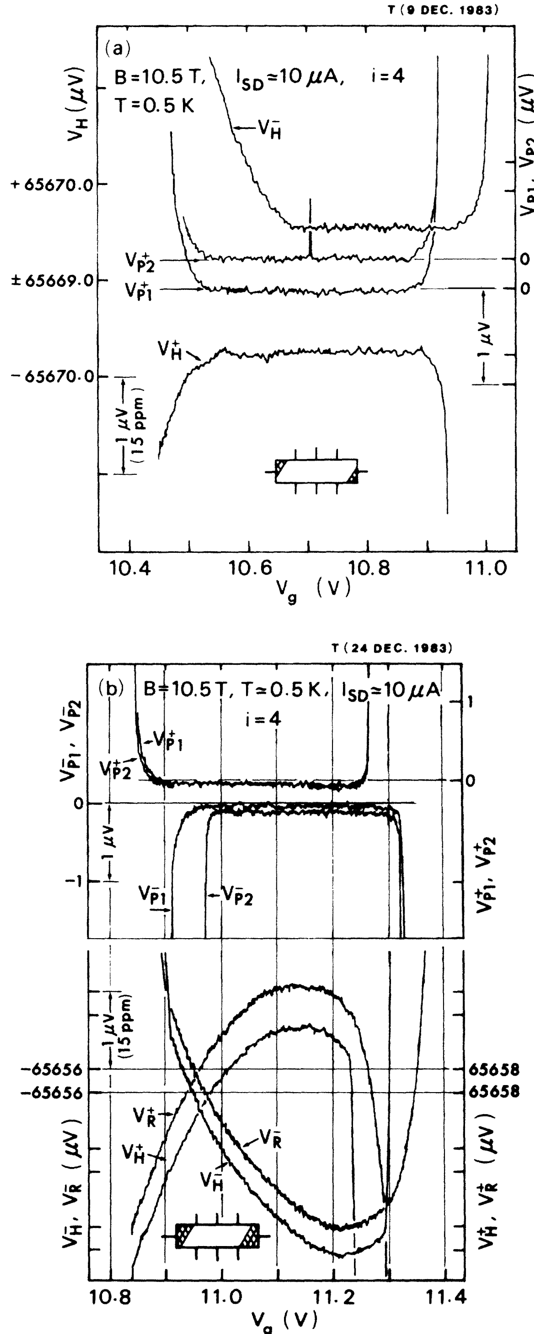

FIG. 16. Different appearances of V_H-vs-V_g curves on the high-precision recorder traces observed for a sample. The insets indicate possible distributions of dissipative regions (hatched areas) schematically. V_{Pj}, voltage drop between P_j and P_j' along the channel; V_R, voltage drop across a 6.45-kΩ resistor; superscripts + and −, polarity of I_{SD}. Sample: T.

IV. RESULTS OF HIGH-ACCURACY MEASUREMENTS

A. Experiments to test flatness of plateaus and accuracy of Eq. (2)

Figure 17 shows the Hall and normal resistances on $i=4$, 8, 12, and 16 plateaus plotted against V_g. The measurements were made at $T \simeq 0.5$ K, $B=10.5$ or 9.0 T, and $I_{SD} \simeq 10$ μA. The plateaus, excluding the $i=16$ plateau, appear to be flat to within 1 mΩ in the range of V_g where $R_{PP'} < 40$ mΩ ($\rho_{xx} < 10$ mΩ) holds for each of these plateaus. Table V lists the range of V_g, the minimum value of ρ_{xx} in the range, and one-standard-deviation uncertainty σ_{n-1} of the average of n measurements of $R_H(i)$ obtained for various values of V_g in the range, while the

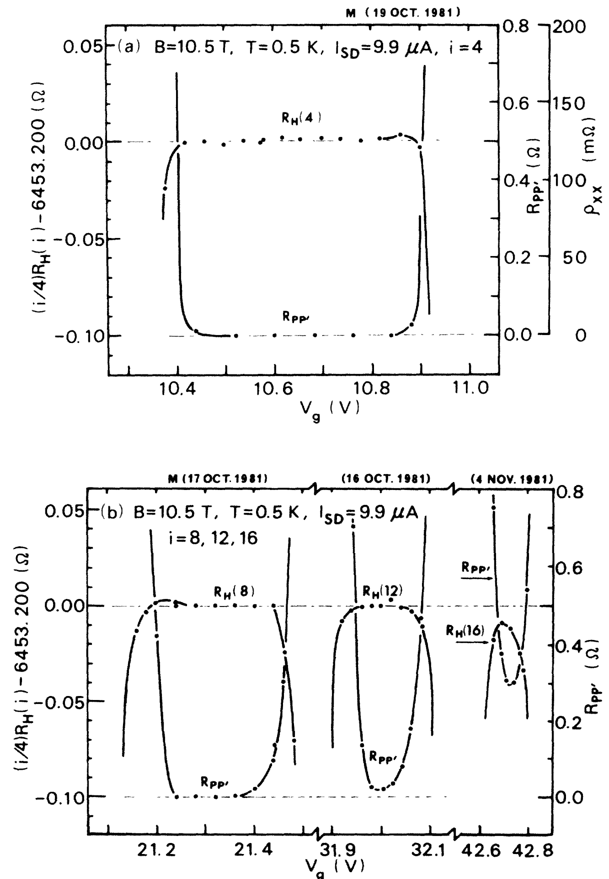

FIG. 17. $R_H(i)$ and $R_{PP'}$ plotted against V_g in plateau regions of $i=4$, 8, 12, and 16, at $T=0.5$ K, $B=10.5$ T, and $I_{SD} \simeq 10$ μA. Sample: M.

TABLE V. Flatness of various Hall plateaus and comparisons of R_H value between different quantum plateaus ($\rho_{xx} < 10$ mΩ). (RSS denotes root-sum-square.)

Date of measurement[a]	i	V_g (V)	$\rho_{xx}^{\min}$ (mΩ)	σ_{n-1} (mΩ)	n	$\frac{iR_H(i)}{4R_H(4)}-1$ (10^{-8})
16–20 Oct. 1981	4	10.46–10.82	0.15	1.1	11	
	8	21.24–21.40	0.19	0.7	6	-7 ± 18
	8	18.20–18.28	0.85	0.6	3	$+5\pm19$
	12	31.98–32.02	5.3	0.9	3	-6 ± 29
31 Jan. 1983	4	12.05	<0.8	1.1	8	
31 Jan. 1983	8	24.05	<0.8	0.2	9	$+6\pm10$
25 Feb. 1983	4	12.18		0.4	8	
25 Feb. 1983	8	23.95		0.4	4	0 ± 10
20 May 1983	4	11.95	<0.6	0.6	9	
21 May 1983	4	11.93		0.9	8	$+1\pm10$
21 May 1983	8	23.55	<0.5	0.3	7	$+8\pm9$
2 June 1983	4	11.95		1.7	18	
2 June 1983	8	23.56		1.0	16	$+10\pm13$
3 Oct. 1983	4	10.85	<1	0.5	5	
4 Oct. 1983	8	21.40	<1	0.3	5	-6 ± 10
Weighted average of data and RSS uncertainty:						
16–20 Oct. 1981 data with 0.15 ppm systematic uncertainty						-2 ± 17
31 Jan.–2 June 1983 data with 0.08 ppm systematic uncertainty						$+4\pm9$

[a]Experimental conditions are given in Table VI.

values of $R_H(i)$ are listed in Table VI.

Comparisons of $R_H(i)$ values between different quantum plateaus have been made. The results, $iR_H(i)/4R_H(4)$, are also listed in Table V together with the one-standard-deviation uncertainty estimated on the basis of the root-sum-square of the individual $\sigma_{n-1}/\sqrt{n}$ values for $R_H(i)$ and the systematic uncertainties. These are ±0.15 ppm and ±0.08 ppm for the Oct. 1981 data and the Jan. through June 1983 data, respectively, as evaluated in Sec. V below. The concentration of 2D electrons in the ith quantized plateau region is given by $n_s \simeq 2.4\times iB\times10^{14}$ m^{-2}: when $B=10.5$ T, $n_s\simeq1\times10^{16}$, 2×10^{16}, and 3×10^{16} for $i=4$, 8, and 12, respectively.

The validity of Eq. (2) is thus experimentally verified to within the accuracy of the present measurement, independent of the quantum number or the concentration of electrons in the inversion layer. This fact suggests that the "constant" in Eq. (2) is unchanged even at the limit of ideal situations where the Hall conductivity is theoretically shown to be quantized exactly to integral fractions of h/e^2, with a possible deviation of less than one part in 10^7 in the case of high-mobility silicon MOSFET's.

B. Reproducibility

Figure 18 shows the values of $R_H(4)$, $2\times R_H(8)$, and $3\times R_H(12)$ plotted against the time at which the measurements were made. The data were obtained under various experimental conditions with different measurement systems which are summarized in Table VI. The error bars denote one-standard-deviation uncertainty σ_{n-1} of the average of n measurements.

In Fig. 18(a) the values of $(i/4)R_H(i)$ are expressed in the ETL as-maintained ohm $\Omega_{\rm ETL}$ based on the calibrations on and before 29 Nov. 1982 and an extrapolation (solid circles), and those on and after 11 Mar. 1983 and extrapolations (open circles). The solid line passes through regions given by $(i/4)\bar{R}_H(i)\pm\sigma_{N-1}/\sqrt{N}$, where the mean values are taken in the respective groups of near-in-time measurements, $N=\sum n$, and n is the number of $R_H(i)$ data. It is noted that the time variation changes abruptly in 1983. The change may have resulted from the following sources: (1) the standard 10-kΩ resistor, (2) the measurement system, (3) as-maintained unit $\Omega_{\rm ETL}$, and (4) the procedure of calibration. However, sources (1) and (2) are found to be less important by comparing Fig. 18(a) with Fig. 18(b) as shown below.

The source (3) also may not be important: According to a recent result of international comparisons [from Nov. 1983 to May 1984, BIPM (Bureau International des Poids et Mesures)], the time variation of 1 $\Omega_{\rm ETL}$ is almost equal to that of $\Omega_{69\text{-BI}}$ and no abrupt change in the value of $\Omega_{\rm ETL}$ has been found between 1977 and 1984.[33] It is thus possible to rule out source (3) as long as the procedure of the comparison has been made with sufficient accuracy.

The same data as shown in Fig. 18(a) are replotted in Fig. 18(b), but the values are obtained on the assumption that the standard 10-kΩ resistor used for the reference is unchanged with time and fixed at a value, e.g., $R_{\rm std}(20)\equiv10\,000.0196$ Ω, the value calibrated on 29 Nov. 1982. The data of May to June 1983 (enclosed in parentheses) are not shown in Fig. 18(a), for simplicity:

TABLE VI. Values corresponding to $h/4e^2$ in chronological order of measurements ($I_{SD} \simeq 10\ \mu A$ unless otherwise noted).

Date	Code of Samples	B (T)	T (K)	i	t (°C)	$(i/4)R_H(i)$ (Ω_{ETL})	(Ω^a)	σ_{n-1} (Ω)	n	Potentiometer, Galvanometer model nos.
23 Mar. '81	Q	14.7	1.4	4	24.2	6453.1992	6453.1873	0.0018	4	9930, 9460A
23 Mar. '81	A	14.7	1.4	4	23.5	6453.1995	6453.1876	0.0023	10	9930, 9460A
23 Mar. '81	B	14.7	1.4	4	23.7	6453.2008	6453.1889	0.0026	8	9930, 9460A
11 Apr. '81	E	10.5	1.3	4	25.0	6453.1995	6453.1881	0.0031	6	9930, 9460A
16 Oct. '81	M	10.5	0.5	12	27.2	6453.2001	6453.1927	0.0027	3	9930, 9829
17 Oct. '81	M	10.5	0.5	8	27.35	6453.2001	6453.1927	0.0014	6	9930, 9829
19 Oct. '81	M	10.5	0.5	4	27.4	6453.2005	6453.1931	0.0011	11	9930, 9829
20 Oct. '81	M	9.0	0.5	8	27.1	6453.2009	6453.1935	0.0011	3	9930, 9829
20 Dec. '82	K	12.0	0.5	4	19.05	6453.2016	6453.2020	0.0016	14	9930, 9829
15 Jan. '83	R	12.0	0.5	4	21.75	6453.2005	6453.2015	0.0008	19	9930, 9829
28 Jan. '83	R	12.0	0.5	4	21.2	6453.2011	6453.2023	0.0008	12	9930, 9829
31 Jan. '83	R	12.0	0.5	4	21.0	6453.2010	6453.2023	0.0011	8	9930, 9829
31 Jan. '83	R	12.0	0.5	8	21.1	6453.2014	6453.2028	0.0005	9	9930, 9829
7 Feb. '83	E	12.0	0.5	4	20.76	6453.2003	6453.2017	0.0008	12	9930, 9829
25 Feb. '83	R	12.0	0.5	4	20.70	6453.2012	6453.2029	0.0004	8	9930, 9829
25 Feb. '83	R	12.0	0.5	8	20.80	6453.2012	6453.2029	0.0008	4	9930, 9829
23 Mar. '83	R	12.0	1.21	4	20.70	6453.2010	6453.2034	0.0006	4	9930, 9829
14 May '83	R	12.0	0.46	4	23.18		6453.2016	0.0008	12	9939, 9829
20 May '83	H	12.0	0.47	4	22.4		6453.2019	0.0006	9	9930, 9829
21 May '83	H	12.0	1.24	4	22.7		6453.2019	0.0009	8	9930, 9829[b]
21 May '83	H	12.0	0.55	8	22.85		6453.2025	0.0008	7	9930, 9829
2 June '83	J	12.0	0.52	4	23.85		6453.2003	0.0007	8	9930, 9829
2 June '83	J	12.0	0.49	8	23.85		6453.2017	0.0012	8	9930, 9829
2 June '83	J	12.0	0.47	4	23.85		6453.2014	0.0012	10	9930, 9829
2 June '83	J	12.0	0.47	8	23.85		6453.2012	0.0016	8	9930, 9829

TABLE VI. (*Continued*).

Date	Code of Samples	B (T)	T (K)	i	t (°C)	$(i/4)R_H(i)$ (Ω_{ETL})	(Ω^a)	σ_{n-1} (Ω)	n	Potentiometer, Galvanometer model nos.
3 Oct. '83	S	10.5	0.5	4	19.94		6453.2074	0.0005	5	9930, 9829[c]
4 Oct. '83	S	10.5	0.5	8	19.94		6453.2070	0.0007	5	9930, 9829[c]
6 Oct. '83	S	10.5	0.5	4	19.94		6453.2077		1	JP, 9460A[d]
23 Dec. '83	T	10.5	0.5	4	20.02		6453.2066		1	JP, SQUID[e]
24 Dec. '83	T	10.5	0.5	4	20.02		6453.2076	0.0006	7	9939, 9829[c,b]
2 Mar. '84	T	10.5	0.5	4	19.89		6453.2084	0.0007	4	9930, 9829[c]
2 Mar. '84	T	10.5	0.5	4	19.89		6453.2078	0.0003	4	9930, 9829[c]
7 Mar. '84	T	10.5	0.5	4	20.03		6453.2088	0.0010	8	9930, 9829[c,b]
16 Mar. '84	U	10.5	0.5	4	19.82		6453.2074	0.0004	12	9930, 9829[c]
12 Apr. '84	U	10.5	0.5	4	19.94		6453.2089	0.0004	4	9930, 9829[c]
13 Apr. '84	U	10.5	0.5	4	19.94		6453.2079	0.0003	5	JP, SQUID[e]

[a]See text and also Fig. 18(b).
[b]$I_{SD} \lesssim 5\ \mu A$.
[c]New system with improved stability in oil-bath temperature (Ref. 47).
[d]Josephson potentiometer (JP) and GI-9460A galvanometer system (Ref. 46).
[e]Josephson potentiometer and SQUID galvanometer system (Refs. 44, 45, and 47).

These data may include a greater systematic error, because the temperature of the standard 10-kΩ resistor (22.7—23.9 °C) is so high compared with t_{cal} that it exceeds the range of correction. The values of $R_{std}(20)$ are also plotted in the figure as deviations (in ppm) from a nominal value 10 000.0000 Ω, to display the time of calibrations on the abscissa and to compare the trend of variation.

In Fig. 18(b) the time variation of $(i/4)R_H(i)$ is caused by that of the standard 10-kΩ resistor, and there is no appreciable change in the slope between 1982 and 1983. It is also noted that no difference is found among the values of $R_H(i)$ obtained by means of different measurement systems. These facts indicate that the abrupt change of $(i/4)R_H(i)$ shown in Fig. 18(a) is not due to that of the 10-kΩ resistor or the measurement systems. That is, the sources (1), (2), and (3) with some reservation are less important in explaining the change. The systematic uncertainty associated with the calibrations of the 10-kΩ resistor against 1 Ω_{ETL} could be greater than that which has been stated.[34] The sources of error in the calibration procedure are open to discussion and reexamination.

We obtain tentative values of $(i/4)R_H(i)$ in Ω_{ETL} on the assumption that (1) the above-mentioned unknown systematic uncertainty is constant for the calibrations on and before 29 Nov. 1982, and (2) thereafter the time variation of the 10-kΩ resistor is −1.2 ppm/year for a few

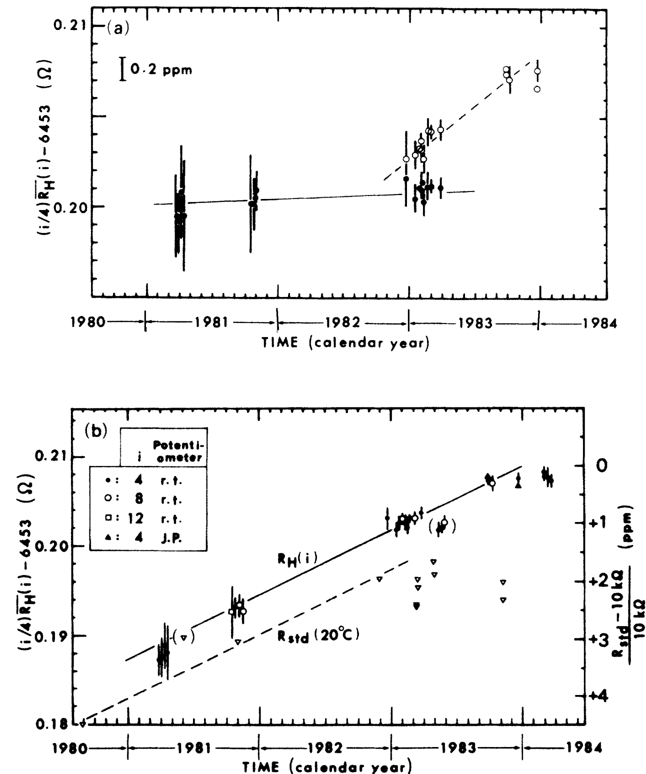

FIG. 18. Long-term observation of $(i/4)R_H(i)$ values expressed in various units. The solid lines pass through the mean values taken within near-in-time measurements, and the dashed lines are meant to guide the eye. Open triangles denote values of $R_{std}(20)$ (see in the text).

TABLE VII. Long-term reproducibility of "h/e^2" values.

Period of measurement	Mean value of N R_H data ($\Omega_{\rm ETL}$)	σ_{N-1} (mΩ)	N	$\sigma_{N-1}/\sqrt{N}$ (mΩ)
23 Mar. '81–11 Apr. '81	6453.1998	2.3	28	0.44
16 Oct. '81–20 Oct. '81	6453.2004	1.3	23	0.28
15 Jan. '83–23 Mar. '83	6453.2009	0.8	76	0.09

months. These values are listed in Table VI, and the average of N data taken within each group of near-in-time measurements is given in Table VII. For the data of 68 days of measurement from 15 Jan. to Mar. 1983 ($N=76$), the values corresponding to h/e^2 are reproduced to within 0.1 ppm. This result indicates that the Hall resistance is stable and reproducible to within a few parts in 10^7 uncertainty, regardless of the experimental conditions tested, shape of samples, and systems for the measurement. The mean value taken from these 76 data and its one-standard-deviation uncertainty are

$$(i/4)\overline{R}_H(i)=6453.2009\pm0.0022\ \Omega_{\rm ETL}(0.34\ \text{ppm})\ , \tag{6}$$

excluding the "unknown" systematic uncertainty associated with the calibration procedure.

V. ASSIGNMENT OF UNCERTAINTIES AND DISCUSSION

A. Random uncertainty

It was reported in a previous paper[15] that the one-standard-deviation uncertainty σ_{n-1} of the average of n data was about 0.3 ppm for measurements with $I_{\rm SD}\simeq10$ μA. The value was reduced to $\sigma_{n-1}\simeq0.1$ ppm for measurements on and after 15 Jan. 1983 by improving the environmental conditions in addition to the time schedule of the measurement. In this case, the major source of σ_{n-1} is the fluctuations in the secondary current of the Guildline 9930 DCC potentiometer. These fluctuations (~0.01 Hz, ~0.2 ppm peak-to-peak) were detected by comparing the time variations of two different output voltages of ~1 and 0 V, which were individually balanced against the emf of a temperature-controlled standard cell and against ±0 V generated from two standard cells connected in series opposition.

The uncertainty in the mean value of N data points is taken to be $\sigma_{N-1}/\sqrt{N}$, provided that the day-to-day scatter in the data points results from random processes. However, it is not self-evident whether the randomness is due to the same kind of sources throughout the measurements. Because of this reason, we did not combine all the "h/e^2" data listed in Table VI. The final 0.03-ppm result given in Table VIII is the random uncertainty which includes the effect of nonreproducible responses in the DCC potentiometer system, which appears to be systematic for short-term measurements and would become random for a sufficiently long period.

B. Systematic uncertainty

Table VIII summarizes the sources of uncertainty associated with the present experimental system when it is operated at $I_{\rm SD}\simeq10$ μA. The following comments apply to the indicated items.

1. Null detector

a. Resolution of the null detector. The minimum voltage difference which can be detected by the use of the present measurement system is estimated at ~3 nV in the presence of ~60 nV peak-to-peak noise voltage, on the basis of the following test. The sources of noise inherent to the present measuring system are the amplifier [~60 nV peak-to-peak (p-p)] and the standard 10-kΩ resistor (~13 nV/$\sqrt{\rm Hz}$ thermal noise). The voltage resolution of the system is estimated using the circuit shown in Fig. 19. Nominally known small voltages $V_{\rm in}$ are measured with the same measurement system and procedure as described in Sec. II. In Fig. 19 the mean values of six to eight readings plotted against $V_{\rm in}$ are also shown; the vertical bars associated with the data points indicate $\pm\sigma_{n-1}/\sqrt{n}$ where $n=6$–8, the statistical uncertainty. This result indicates that there is no nonreproducible response in sensitivity near zero down to $\sim\frac{1}{20}$ of ~60 nV p-p noise level. The uncertainty associated with this source is considered to be random if the number of measurements is sufficiently large.

b. Zero drift in the null detector. Because the zero drift in the LN-9829 linear amplifier is small, we did not monitor the zero for every measurement. Instead, in some runs the zero drift was recorded together with the V_H and V_R data on a strip-chart recorder. Based on this observation, the uncertainty due to the zero drift is estimated to be 0.02 ppm.

2. Variations in thermal emf's

As a result of improvement in the temperature environment, as described in Sec. II C, the drift of thermal emf's is less than 50 nV for 4 h and almost a linear function of time. Roughly 50% of the thermal emf drift could not be canceled for a measurement of 15 min duration (one set, six readings), which was required to obtain one data point of R_H. Based on this observation, the uncertainty associated with the drift of thermal emf's is assigned as 0.03 ppm.

TABLE VIII. Sources of uncertainty in "h/e^2" measurement.

Sources of uncertainty	Uncertainty (1σ in ppm)
(A) Random uncertainty of the mean, before|since Jan. '83	0.1|0.03
(B) Systematic uncertainty	
(1) Null detector	
(a) Resolution	random[a]
(b) Zero drift	0.02
(2) Variations in thermal emf's	0.03
(3) Variations in measuring currents	
(a) Fluctuations in potentiometer current	random[a]
(b) Long-term drift in potentiometer current	~ 0
(c) Variation in I_{SD}, before|since Jan. '83	<0.1|0.03
(4) Linearity of potentiometer current	
(a) Dial reading	0.03
(b) Power coefficient	0.02
(5) Circuit isolation	0.03
(6) Variations in oil-bath temperature	
(a) Short-term variation	0.03
(b) Long-term variation	0.1
(7) Standard 10-kΩ resistor	
(a) Thermal hysteresis, before|since Jan. '83	0.2|0.05
(b) Calibration data interpolation|extrapolation Oct. '81|(Dec. '82—Mar. '83)	0.05|0.1
(c) Standard 10-kΩ resistor calibration	$0.1\pm x$[b]
(8) Possible Ω_{ETL} shift before|after Jan. '82	0.1|0.2
(9) Possible error of unknown origin indicated by Josephson potentiometer	0.2
(10) Ω_{ETL}/Ω_{SI}	0.4
RSS [random and systematic 1—6(a)], before|since Jan. '83 (for comparisons between different plateau values)	0.15|0.08
RSS [random and systematic 1—9], Oct. '81|(Dec. '82—Mar. '83) (h/e^2 in Ω_{ETL})	0.38|$0.34\pm y$[b]
RSS [random and systematic 1—10], Oct. '81|(Dec. '82—Mar. '83) (h/e^2 in Ω_{SI})	0.55|$0.52\pm z$[b]

[a]Included in (A).
[b]Unknown systematic uncertainty (Sec. IV B).

3. Variations in measuring currents

a. Fluctuations in potentiometer current. The variation in the current of the GI-9930 DCC potentiometer mostly results from random fluctuations and is included in the random uncertainty, as described in subsection A.

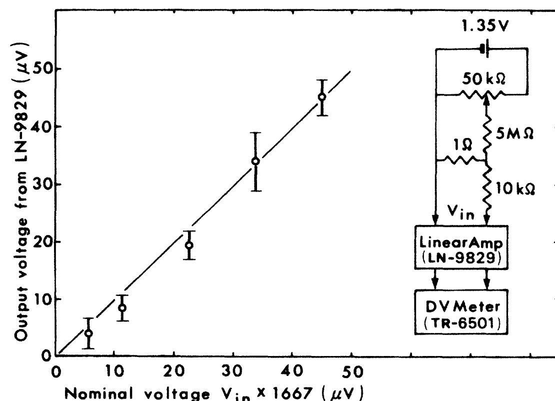

FIG. 19. Circuit for checking the voltage resolution of the measurement system and the result.

b. Long-term drift in potentiometer current. The effect of long-term drift is negligible compared with the time required to complete a set of measurements ($\lesssim 15$ min). The stability of the current is stated to be 1 ppm/day.

c. Variation in I_{SD}. A change in I_{SD} is caused by the variation in emf of the channel-current source (11 mercury batteries). This variation is found to be ~ 40 ppm/deg using the present oil bath. Because the oil-bath temperature changes almost linearly with time and the change is less than ± 0.03 °C for 4 h, the effect of temperature drift is approximately eliminated by regulating the measurement sequence. The uncertainty associated with this source comes from the nonlinear time drift and an increase in time interval caused by delay of the emf measurement behind the scheduled time, and is estimated at 0.03 ppm.

4. Linearity of the potentiometer

In order to compare the values of $R_H(i)$ between different quantum plateaus, it is required to measure different voltages (with a constant I_{SD}) associated with different i values: ~ 21 mV for $i=12$, ~ 32 mV for $i=8$,

$\sim$64 mV for $i=4$, and $\sim$100 mV for the standard 10-kΩ resistor.

a. Dial reading. Because the linear dependence of the secondary current on the measuring dials of the Guildline 9930 DCC potentiometer can be self-checked, the correction to the dial reading was made once in several months. The uncertainty associated with the dial to current linearity comes from the uncorrected residues and the drift between the successive self-checking, and is estimated at 0.03 ppm.

b. Power coefficient. Another source of error is the power coefficient of the emf-generating resistor through which the secondary current of the DCC potentiometer flows. The secondary current is changed from 21 to 100 mA and the difference in power dissipation causes a nonlinearity of the emf output. We made a measurement to determine and correct this error using three standard 1-Ω resistors connected in series, and applying a constant current of $\sim$50 mA which is supplied from the primary circuit of the current comparator, on the assumption that the secondary current is exactly proportional to the dial reading. The result of measurements yields the value of voltage V, which is to be obtained at the limit of zero-power coefficient, against the dial reading V_D as $V/V_D=1+\beta V_D^2$, where $\beta=(+0.074\pm0.022)\times10^2$ ppm/V^2 for the DCC potentiometer used. Based on this measurement the following corrections for the power coefficient were applied to the ratios of $V_H(i)/V_R$, where $R=10$ kΩ, for the present measurement with $I_{SD}=9.9$ μA, on the $\times0.1$ (0.2 V) range: -0.04 ± 0.01 ppm for $V_H(4)/V_{10\,k\Omega}$, -0.06 ± 0.02 ppm for $V_H(8)/V_{10\,k\Omega}$, and -0.07 ± 0.02 ppm for $V_H(12)/V_{10\,k\Omega}$.

5. Circuit isolation

The effect of circuit leakage current has been estimated in three ways:

(1) The individual leakage paths are measured directly as described in Sec. II C by applying a dc voltage of $\sim$10 V exclusive of the lowest part of the sample holders which are cooled to below 1 K when they are used. In the course of this measurement, we observed leakage currents which required several hours to attain equilibrium values and were likely to be due to the dielectric polarization of the insulation as discussed by Finnegan, Denenstein, and Langenberg.[35] Therefore, we made leakage measurements 2–3 min after the circuit had been closed. This time interval corresponds to the balancing time of I_{SD} after a polarity reversal in the measurements. In order to minimize the effect of polarization currents, the gate voltage was applied about 1 h prior to the first run of high-accuracy measurements, and circuits and apparatus which were not in use were all removed from the measurement circuit. The overall leakage resistance obtained is greater than 10^{12} Ω between the circuit and ground. Based on this result the uncertainty associated with the leakage current is less than 0.02 ppm.

(2) The gate voltage ranges from 10 to 50 V for the present measurements and the voltage level is 100–500 times as high as those of other circuits. The electrical insulation has been tested at the highest gate voltages to be applied, and found to be greater than 2×10^{12} Ω between the gate supply and return leads. The insulation is greater by one more order of magnitude between the gate-voltage-supplying circuit and the other leads. The error due to the leakage current from the gate circuit to the other circuit is considered to be equivalent to that due to thermal emf's, provided the gate voltage and the distribution of the leakage current is unchanged during the measurement of V_H and V_R. That is, the error can be canceled by reversing the direction of I_{SD}, except for the part which results from the change of the electric potential distribution in the sample on I_{SD} reversal; the change is $2V_{SD}$, at most, for the measurement in which the V_g reference point is fixed at one of the S-D electrodes (see Sec. II D). Since $2V_{SD}\simeq 2R_H I_{SD}\simeq 130$ mV in the present case, the change in the distribution of the leakage current from the gate circuit is less than (130 mV)/(2×10^{12} Ω), and the uncertainty associated with this source is less than 0.01 ppm.

(3) We compared two values of $R_H(4)$ obtained from measurements for two samples, 44-4-11-L ($\delta=800$ nm) and 72-17H53-20-$L1$ ($\delta=200$ nm), for which $i=4$ plateaus under $B=12$ T occurred at $V_g=41.0$ and 10.7 V, respectively. The difference is found to be (-0.09 ± 0.09) ppm as calculated from the data listed in Table VI and a systematic uncertainty of 0.08 ppm (given in Table VIII). No significant leakage effect is observed in the gate circuit up to $V_g=41.0$ V.

On the basis of these leakage measurements, the uncertainty associated with the circuit insulation is less than 0.03 ppm.

6. Variation in oil-bath temperature and reading error of thermometers

a. Short-term variation. For short-term measurement such as a comparison of $R_H(i)$ values between different plateaus, the stability of the oil-bath temperature determines the accuracy of the result. By selecting the period of the measurement, the oil-bath temperature was made stable to within $\pm0.03\,^\circ$C for $\sim$4 h. Based on the temperature coefficient of the standard 10-kΩ resistor, the uncertainty from this source is estimated at 0.03 ppm.

b. Long-term variation. The temperature of the standard 10-kΩ resistor was monitored with a mercury-in-glass thermometer calibrated at 20 °C, as well as with a thermistor. The reading error of the mercury-in-glass thermometer is $\pm0.05\,^\circ$C and this yields an uncertainty of ±0.06 ppm in the value of $R_{std}(t)$ due to the temperature coefficient of the 10-kΩ resistor. The temperature difference between the top and the base of the 10-kΩ resistor is 0.03 °C, and this value does not change with time. Since the measurements were made without intentionally controlling the temperature of the 10-kΩ resistor, t, the values of t are usually not equal to the temperature of calibration, t_{cal}. In order to keep the error due to the temperature correction below 0.1 ppm, we have chosen the range of the oil-bath temperature so that $|t-t_{cal}|<4\,^\circ$C, for high-accuracy measurements. The uncertainty from these sources is estimated to be 0.1 ppm.

7. Standard 10-kΩ resistor

a. Thermal hysteresis. A long thermal time constant of the standard 10-kΩ resistor and covering case can be a source of uncertainty when the oil-bath temperature varies. The uncertainty is evaluated from a shift in $R_H(4)$ value which is observed as the oil-bath temperature drifts: ±0.15 ppm for a temperature rise of 0.1 °C/h. From this result, the uncertainty is estimated at 0.2 ppm for the data obtained in and before 1982, and 0.05 ppm for those obtained in and after Jan. 1983.

b. Interpolation and/or extrapolation of calibration data. On the assumption that the time variation of $R_{\rm std}(t)$ is linear, the value is obtained from interpolation and/or extrapolation between successive calibrations. The uncertainty varies depending on the time interval from the nearest date of calibration. The uncertainty from this source is estimated by analyzing the trend of time variation: it is 0.05 ppm for the measurements carried out in Oct. 1981 and 0.1 ppm for those during Dec. 1982 through Mar. 1983.

c. Calibration of standard 10-kΩ resistor. The resistor has been calibrated by the Electrical Standards Section, ETL. The uncertainty associated with the calibration procedure is stated to be 0.1 ppm;[33] however, the "unknown" sources of systematic uncertainty (Sec. IV B) should be taken into account.

8. Possible shift of Ω_{ETL} from 1979-1980 value

If the "unknown" uncertainty is regarded to be constant, which is what is supposed to occur when the meausrements are made under the same condition by the same single operator, then the solid line in Fig. 18(a) indicates a possible drift of the ETL ohm since the international comparisons were performed between 1979 and 1980.[30,36] This source is supposed to contribute uncertainties of ~0.1 ppm for the runs in 1981 and ~0.2 ppm for the runs in 1983.

9. Possible error of unknown origin indicated by Josephson potentiometer

A constant difference, ~0.2 ppm, is observed between the values of $R_H(4)$ obtained by means of the present system and a new system as described in subsection C 3 below.

10. Ω_{ETL}/Ω_{SI}

It has been reported that 1 $\Omega_{\rm ETL}=1$ $\Omega_{\rm SI}$ with an uncertainty of 0.4 ppm.[34]

C. Discussion

1. Random uncertainty resulting from ampere-turn noise

The values of quantized Hall resistance for individual runs which were performed during the period Jan. to Mar. 1983 are considered to be of the same quality with regard to the sources of uncertainty, σ_{n-1} in Table VI, because the environment, system, and procedure of the measurement were kept essentially unchanged over the period. Therefore, we take the simple average of 76 data obtained in this period as the mean value of R_H, which is given in the last line of Table VII, together with σ_{N-1} and $\sigma_{N-1}/\sqrt{N}$, where $N=76$. The value of $\sigma_{N-1}/\sqrt{N}$ is assigned as the one-standard-deviation random uncertainty of the mean value of R_H, if the data scattering results from the same kind of random processes throughout the runs.

However, as seen in Table VI, the values of σ_{n-1} for various different runs differ considerably from each other. We examine the consistency of the above 76 data (eight runs) after Taylor as follows:[37] Since the change in environment is very small for the duration of one run, the scattering of data within the run is considered to be due to a random process, and one-standard-deviation random uncertainty σ_j for the jth run is given by $\sigma_{n-1}^j/\sqrt{n}$, where n is the number of data and σ_{n-1}^j the one standard deviation of the run. The error determined by internal consistency σ_I and that determined by external consistency σ_E are calculated as

$$\sigma_I^2=\left[\sum_{j=1}^{M}\sigma_j^{-2}\right]^{-1}=(0.011\ \text{ppm})^2$$

and

$$\sigma_E^2=\left[\sum_{j=1}^{M}(X_j-\bar{X})^2/\sigma_j^2\right]\Bigg/\left[(M-1)\sum_{j=1}^{M}\sigma_j^{-2}\right]$$

$$=(0.024\ \text{ppm})^2\ ,$$

respectively. Here, $M=8$, $\bar{X}$ denotes the usual weighted average given by

$$\bar{X}=\left[\sum_{j=1}^{M}(X_j/\sigma_j^2)\right]\Bigg/\left[\sum_{j=1}^{M}\sigma_j^{-2}\right]\ ,$$

and X_j the average values of $R_H(4)$ or $2R_H(8)$ data in the jth run. The Birge ratio $R_B\equiv\sigma_E/\sigma_I$ in this case is larger than one, $R_B=2.2$, i.e., the statistic chi-squared $\chi^2=(M-1)R_B^2=34$ for $M-1=7$ degrees of freedom. This result implies that the data are highly inconsistent with the assumption that the data scattering between different runs and that in each individual run are both subjected to the same kind of random processes.

The same inconsistency in the chi-squared test has been observed also in the runs carried out after Oct. 1983 where both the temperature in the oil bath and of the environment have been intentionally controlled so as to be constant. Therefore, it is not possible to attribute the inconsistency to a systematic error resulting from the day-to-day difference in environmental conditions. The inconsistency is considered to be caused by the DCC potentiometer and null-detector system. However, the null detector must have contributed little, because the amplitude of internal noise and drifts had been ascertained to be unchanged throughout the eight runs. The DCC potentiometer thus can be the source of systematic error or spuriously small σ_j values.

In the present DCC potentiometer system, a nonreproducible response of the secondary current has been ob-

served sometimes against a small change in ampere turns of the primary current, which corresponds to 30% of one step in the dial of the smallest digit. The error in the Hall voltage from this source is estimated at 0.05 ppm for $i=4$ plateaus and 0.1 ppm for $i=8$ plateaus when $I_{SD}\simeq 10\ \mu A$, and is of the same voltage level as the current-comparator noise.[38] The observed feature can be caused by a hysteresis of the magnetic core in the current comparator, which possibly results from friction in the motion of magnetic domains.

The effect of this nonreproducibility is to add (or subtract) some small values to (or from) the measurement results. The values sometimes remain constant for the duration of one or two runs. However, the values are essentially random in sign and magnitude, and should amount to an average of ~ 0, when the observation is repeated a sufficiently large number of times with long time intervals between measurements. This fact indicates that for a single measurement $(n=1)$ of $R_H(i)$, the lowest limit of uncertainty is determined by that associated with the nonreproducibility effect when a current-comparator-type potentiometer is used. That is, σ_j is considered to be given by

$$\sigma_j^2=(\sigma_{n-1}^j)^2/n+(0.05\ \text{ppm})^2$$

for $R_H(4)$ and

$$\sigma_j^2=(\sigma_{n-1}^j)^2/n+(0.1\ \text{ppm})^2$$

for $R_H(8)$, resulting in $\sigma_I=0.024$ ppm, $\sigma_E=0.022$ ppm, $R_B=0.9$, and $\chi^2=5.7$. The one-standard-deviation random uncertainty is thus evaluated as 0.03 ppm (0.17 mΩ) for the eight runs while the weighted average of $R_H(4)$ and $2\times R_H(8)$ obtained is the same as the value given in Table VII.

2. *Possible deviations from h/e^2*

According to the result described in Sec. III C, there should be no problem in achieving an experimental situation under which the relative deviation of ρ_{xy} from an ideal value becomes less than 0.01 ppm, if the empirical relation, Eq. (5), holds in the region of smaller ρ_{xx}. This is expected from the result obtained by Cage *et al.*, for GaAs-$Al_xGa_{1-x}As$ heterostructures.[28] On the other hand, other sources of the ρ_{xy}-value deviation are also considered to exist.

It has been found for silicon MOSFET samples at $T\lesssim 0.3$ K, $B=12$ T, and $I_{SD}\lesssim 10^{-7}$ A rms (10–20 Hz) that random peaked structures are superimposed on both V_H-versus-V_g and $V_{PP'}$-versus-V_g curves. The structures are characterized by the following: (1) the gate voltages where the peaks and dips occur are independent of temperature and values of I_{SD} for a single sample, (2) the amplitude of the random structure increases as the temperature is lowered and as the values of I_{SD} and/or V_g are decreased, e.g., the amplitude attains 30% of the value of $V_{PP'}$ at $V_g\simeq 5$ V, $I_{SD}\simeq 10^{-8}$ A, and $T\simeq 10$ mK, and (3) the amplitude is almost independent of the magnetic field strength.[39] Similar structures have been observed by Tidey, Stradling, and Pepper[40] and Cole, Lakhani, and Stiles[41] in the differential conductance of silicon MOSFET devices at higher temperatures, and also by von Klitzing[42] in GaAs-$Al_xGa_{1-x}As$ heterostructures. Although the effect of the random peaked structures is not observed under the conditions of the present measurement, it might limit the precision (or the flatness of the Hall-resistance plateaus) when the resolution of the measurement is improved to the order of 10^{-8} or better.

When the contact areas of the Hall-potential probes are not on the channel edges, but inside the channel, one would obtain a spurious value of $\rho_{xy}(i)$ and also deformed Hall plateaus on a recorder trace of V_H versus V_g (or B) at V_g's (or B's) where $\sigma_{xx}\simeq 0$ holds over the channel. In this case, the contact areas are surrounded by a dissipationless region (like the center of a Corbino disk), and the circuit for the Hall-voltage measurement which includes these potential probes and the amplifier becomes effectively open. The sign and magnitude of the spurious output voltages from the amplifier vary depending on the value of σ_{xx} and input offset current in the amplifier. This case is easily distinguished by a strong temperature dependence (via σ_{xx}) of the shape of the V_H-versus-V_g (or -B) curve in the plateau region. If the value of ρ_{xy} becomes unstable or the data scatter increases as the temperature is lowered in spite of a small ρ_{xx} value, this effect should be taken into account.

3. *Need for improvement in linearity and resolution*

The uncertainty of the present experiment is eventually determined by the linearity of a potentiometer which generates odd voltage ratios such as 10:6.45, the power coefficient of the potentiometer, and the resolution of a galvanometer. The uncertainty resulting from these sources is $\lesssim 0.1$ ppm, and will not be improved further as long as the measurement is made using $I_{SD}\simeq 10\ \mu A$ and a measurement system operated at room temperature.

For this reason, a new technique is necessary for the voltage comparison with an order- (or orders-) of-magnitude improved resolution and linearity. We have undertaken an attempt on the basis of a Josephson potentiometer and superconducting quantum-interference device (SQUID) galvanometer system which is essentially free from the linearity and power-coefficient problem.[43,44] As a very preliminary result, a constant difference has been observed between the values of $R_H(4)$ obtained by means of the new system[45] and the conventional (present) system as follows: for 10:6.45 comparison,

$$(V_{6.45\,k\Omega}/V_{10\,k\Omega})_N/(V_{6.45\,k\Omega}/V_{10\,k\Omega})_C-1=(-0.24\pm 0.11)\text{ppm}$$

using $I_{SD}\simeq 10\ \mu A$ and

$$[V_H(4)/V_{10\,k\Omega}]_N/[V_H(4)/V_{10\,k\Omega}]_C-1=(-0.22\pm 0.15)\ \text{ppm}$$

using $I_{SD}\simeq 5\ \mu A$; for 6.45:6.45 comparison,

$$[V_H(4)/V_{6.45\,k\Omega}]_N/[V_H(4)/V_{6.45\,k\Omega}]_C-1=(-0.16\pm 0.06)\ \text{and}\ (-0.22\pm 0.06)\ \text{ppm}$$

using $I_{SD}\simeq 10\ \mu A$. Here, $V_{6.45\,k\Omega}$ and $V_{10\,k\Omega}$ are the

voltage drops across the 6.45- and 10-kΩ reference resistors, and the subscripts N and C denote the new and conventional systems, respectively.

The origin of this discrepancy is partly a tracking error of the Guildline potentiometer (described in subsection C 1). Although the other major part is still unknown, the above result indicates that the linearity error of the Guildline potentiometer contributes little to the discrepancy since the same ~0.2-ppm difference is observed even in the 6.45:6.45 comparison, and sources associated with the silicon MOSFET sample and the circuit which are contained in a cryostat may be less important since the ~0.2-ppm difference is also observed in the comparison between two reference resistors, the cryostat being eliminated. On the other hand, the drift of the thermal emf's in the circuits of the Josephson potentiometer and the SQUID galvanometer, which are contained in two separate, relatively small cryostats, may be important. Thus, it is not clear, as yet, whether the discrepancy comes from the new system or the conventional system. We include this unexplained systematic error in Table VIII as "possible error of unknown origin indicated by Josephson potentiometer."

VI. CONCLUSION

The following conclusions are derived from the present results:

(1) The value of $\rho_{xy}(i)$ for the ith quantized Hall plateau is verified to be constant provided the measurement is carried out under the condition that $\rho_{xx} < (4/i) \times 10^{-2}$ Ω. That is, the value corresponding to h/e^2 is independent of the electron concentration, temperature, magnetic field strength, and channel current, to within 0.1 ppm, the accuracy of the present experiment; the effect of electron-electron interactions on the value of ρ_{xy} is not found at concentrations from 1×10^{16} to 3×10^{16} m^{-2}.

(2) The value of $\rho_{xy}(i)$ and its one-standard-deviation uncertainty obtained are $(i/4)\overline{R}_H(i) = 6453.2009 \pm 0.0022$ $\Omega_{\rm ETL}$, and the corresponding values for the fine-structure constant are $\alpha^{-1} = 137.035\,978 \pm 0.000\,072$, temporarily excluding the "unknown" systematic uncertainty described in Sec. IV B.

(3) The effect of dissipative regions on the value of ρ_{xy} is negligible to within a few parts in 10^7 as long as the condition for a vanishingly small ρ_{xx} value given in (1) above is satisfied.

(4) For the measurement of ρ_{xy} with improved accuracy, less than a few parts in 10^8 uncertainty, the presence of dissipative regions is undesirable because it would cause in effect a reduced aspect ratio for the channel and $(1/f)$-type noise or fluctuations in $I_{\rm SD}$. The latter problem is discussed elsewhere.[46]

(5) Non-thermal-equilibrium electrons are considered to be generated in these dissipative regions and to diffuse along the channel, resulting in an increase of ρ_{xx}. For every step of the accuracy improvement, the effect of these electrons on ρ_{xy} should be reexamined by comparing the results for various $I_{\rm SD}$ values. On the other hand, the shape and dimensions of the channel should be devised in order to reduce the effect of these electrons.

(6) The technique developed to measure the quantum Hall effect to the limit of highest precision and accuracy can be utilized for experiments at the lowest excitation, such as quantum-mechanical diffusion of electrons through a random medium, or to examine scaling theories of localization.[47–49]

ACKNOWLEDGMENTS

The authors would like to thank Dr. T. Dai for preparing reference resistors, Dr. H. Sakurai for calibration of a standard platinum-resistance thermometer, and Professor S. Tanuma, Professor K. Hara, and Dr. M. Morimura for stimulating discussions. The authors are grateful to K. Murakami, H. Nishinaka, and T. Igarashi in calibrating the standard 10-kΩ resistor. They are grateful to T. Nemoto for his continuous encouragement.

[1]A. B. Fowler, F. F. Fang, W. E. Howard, and P. J. Stiles, Phys. Rev. Lett. **16**, 901 (1966).

[2]H. L. Störmer, R. Dingle, A. C. Gossard, E. Wiegmann, and M. D. Sturge, Solid State Commun. **29**, 705 (1979).

[3]Y. Guldner, J. P. Vieren, P. Voisin, and M. Voos, Appl. Phys. Lett. **40**, 877 (1982).

[4]K. von Klitzing, G. Dorda, and M. Pepper, Phys. Rev. Lett. **45**, 494 (1980).

[5]T. Ando, Y. Matsumoto, and Y. Uemura, J. Phys. Soc. Jpn. **39**, 279 (1975).

[6]S. Kawaji and J. Wakabayashi, in *Physics in High Magnetic Fields*, Vol. 24 of *Springer Series in Solid-State Sciences*, edited by S. Chikazumi and N. Miura (Springer, New York, 1981), p. 284.

[7]E. Braun, E. Staben, and K. von Klitzing, Physikalisch-Technische Bundesanstalt—Mitteilungen **90**, 350 (1980).

[8]R. E. Prange, Phys. Rev. B **23**, 4802 (1981).

[9]H. Aoki and T. Ando, Solid State Commun. **38**, 1079 (1981).

[10]D. J. Thouless, J. Phys. C **14**, 3475 (1981).

[11]R. B. Laughlin, Phys. Rev. B **23**, 5632 (1981).

[12]B. I. Halperin, Phys. Rev. B **25**, 2185 (1982).

[13]Y. Imry, J. Phys. C **15**, L221 (1982).

[14]P. Středa, J. Phys. C **15**, L717 (1982).

[15]C. Yamanouchi, K. Yoshihiro, J. Kinoshita, K. Inagaki, J. Moriyama, S. Kawaji, T. Endo, M. Koyanagi, K. Murakami, T. Igarashi, and A. Nakamura, in *Precision Measurement and Fundamental Constants II*, edited by B. N. Taylor and W. D. Phillips, National Bureau of Standards Spec. Publ. No. **617**, (U.S. GPO, Washington D.C., 1984), p. 529; K. Yoshihiro, J. Kinoshita, K. Inagaki, C. Yamanouchi, J. Moriyama, and S. Kawaji, Surf. Sci. **113**, 16 (1982).

[16]D. C. Tsui and A. C. Gossard, Appl. Phys. Lett. **38**, 550 (1981).

[17]D. C. Tsui, A. C. Gossard, B. F. Field, M. E. Cage, and R. F. Dziuba, Phys. Rev. Lett. **48**, 3 (1982).

[18]L. Bliek, E. Braun, H. J. Engelmann, H. Leontiew, F. Mel-

chert, W. Schlapp, B. Stahl, P. Warnecke, and G. Weimann, Physikalisch-Technische Bundesanstalt—Mitteilungen 93, 21 (1983).

[19]E. R. Williams and P. T. Olsen, Phys. Rev. Lett. **42**, 1575 (1979).

[20]T. Kinoshita and W. B. Lindquist, Phys. Rev. Lett. **47**, 1573 (1981).

[21]K. Yoshihiro, J. Kinoshita, K. Inagaki, C. Yamanouchi, J. Moriyama, and S. Kawaji, J. Phys. Soc. Jpn. **51**, 5 (1982).

[22]Preliminary reports of this work have appeared in Ref. 21 and K. Yoshihiro, J. Kinoshita, K. Inagaki, C. Yamanouchi, J. Moriyama, and S. Kawaji, Physica **117&118B**, 706 (1983).

[23]A. Yagi, Ph.D. thesis, Gakushuin University, 1980.

[24]K. Murakami (private communication).

[25]When the center of a Hall plateau does not coincide with the minimum of the ρ_{xx}-versus-V_g curve on the V_g axis, the measurement of R_H should be made at the value of V_g where ρ_{xx} drops to the minimum value. This is because 2D electrons under different V_g's (or B's) are in different states: $\rho_{xx}(V_{g1})$ and $\rho_{xy}(V_{g2})$ are elements of different resistivity tensors individually, unless $V_{g1}=V_{g2}$.

[26]K. I. Wysokiński and W. Brenig, Z. Phys. B **54**, 11 (1983).

[27]H. J. Lippmann and F. Kuhrt, Z. Naturforsch. **13a**, 462 and 474 (1958).

[28]M. E. Cage, B. F. Field, R. F. Dziuba, S. M. Girvin, A. C. Gossard, and D. C. Tsui, Phys. Rev. B **30**, 2286 (1984).

[29]M. E. Cage, R. F. Dziuba, B. F. Field, E. R. Williams, S. M. Girvin, A. C. Gossard, D. C. Tsui, and R. J. Wagner, Phys. Rev. Lett. **51**, 1374 (1983).

[30]S. Kawaji, in *Foundations of Quantum Mechanics in the Light of New Technology,* proceedings of the International Symposium, Tokyo, edited by S. Kamefuchi *et al.* (Central Research Laboratory, Hitachi, Ltd., Kokubunji, Tokyo, 1983), p. 327.

[31]J. Kinoshita, K. Inagaki, C. Yamanouchi, K. Yoshihiro, J. Moriyama, and S. Kawaji, in *Application of High Magnetic Fields in Semiconductor Physics,* Vol. 177 of *Lecture Notes in Physics,* proceedings of the International Conference, Grenoble, edited by G. Landwehr (Springer-Verlag, Berlin, 1983), p. 33.

[32]B. Eitan, D. Frohman-Bentchkowsky, J. Shappir, and M. Balog, Appl. Phys. Lett. **40**, 523 (1982).

[33]H. Nishinaka and T. Igarashi, in Digests of the 45th Annual Meeting of the Japan Society of Applied Physics, Okayama University, Okayama, 1984, p. 17 (in Japanese) (unpublished).

[34]G. Leclerc, Metrologia **14**, 171 (1978); ETL News No. 328 (1977); No. 349 (1977) (in Japanese).

[35]T. F. Finnegan, A. Denenstein, and D. N. Langenberg, Phys. Rev. B **4**, 1487 (1971).

[36]J. Kinoshita, K. Inagaki, C. Yamanouchi, K. Yoshihiro, J. Moriyama, and S. Kawaji, Document No. CCE/83-19, submitted to 16th Session of the Comité Consultatif d'Electricité, (Bureau International des Poids et Mesures, 1983, in press).

[37]B. N. Taylor, W. H. Parker, and D. N. Langenberg, *The Fundamental Constants and Quantum Electrodynamics,* 2nd ed. (Academic, New York, 1970).

[38]M. P. MacMartin and N. L. Kusters, IEEE Trans. Instrum. Meas. **IM-17**, 263 (1968).

[39]J. Kinoshita and K. Yoshihiro, Bussei Kenkyu **40**, No. 4, Suppl., 110 (1983).

[40]R. J. Tidey, R. A. Stradling, and M. Pepper, J. Phys. C **7**, L353 (1974).

[41]T. Cole, A. A. Lakhani, and P. J. Stiles, Surf. Sci. **58**, 56 (1976).

[42]K. von Klitzing (private communication).

[43]M. Koyanagi, T. Endo, and A. Nakamura, in *Precision Measurement and Fundamental Constants II,* Ref. 15, p. 489.

[44]T. Endo, M. Koyanagi, and A. Nakamura, IEEE Trans. Instrum. Meas. **IM-32**, 267 (1983).

[45]J. Kinoshita, K. Inagaki, C. Yamanouchi, K. Yoshihiro, T. Endo, Y. Murayama, M. Koyanagi, J. Moriyama, J. Wakabayashi, and S. Kawaji, in *Foundations of Quantum Mechanics in the Light of New Technology,* Ref. 30, p. 339.

[46]K. Yoshihiro, J. Kinoshita, K. Inagaki, C. Yamanouchi, Y. Murayama, T. Endo, M. Koyanagi, J. Wakabayashi, and S. Kawaji, Surf. Sci. (to be published).

[47]J. T. Edwards and D. J. Thouless, J. Phys. C **5**, 807 (1972).

[48]E. Abrahams, P. W. Anderson, D. C. Licciardello, and T. V. Ramakrishnan, Phys. Rev. Lett. **42**, 673 (1979).

[49]T. Ando and H. Aoki, J. Phys. Soc. Jpn. **54**, 2238 (1985).